

Geologica Acta: an international earth science journal

ISSN: 1695-6133

geologica-acta@ictja.csic.es

Universitat de Barcelona España

GARCÍA-MORENO, O.; CORRETGÉ, L. G.; HOLTZ, F.; GARCÍA-ARIAS, M.; RODRÍGUEZ, C.

Phase relations in the Cabeza de Araya cordierite monzogranite, Iberian Massif: implications for the formation of cordierite in a crystal mush Geologica Acta: an international earth science journal, vol. 15, núm. 4, diciembre, 2017, pp. 337-359 Universitat de Barcelona

Barcelona, España

Available in: http://www.redalyc.org/articulo.oa?id=50553843007



Complete issue

More information about this article

Journal's homepage in redalyc.org



Scientific Information System

Network of Scientific Journals from Latin America, the Caribbean, Spain and Portugal Non-profit academic project, developed under the open access initiative

# Phase relations in the Cabeza de Araya cordierite monzogranite, Iberian Massif: implications for the formation of cordierite in a crystal mush

O. GARCÍA-MORENO<sup>1,2</sup> L. G. CORRETGÉ<sup>1</sup> F. HOLTZ<sup>3</sup> M. GARCÍA-ARIAS<sup>4</sup> C. RODRÍGUEZ<sup>5</sup>

#### <sup>1</sup>Departmento de Geología, Universidad de Oviedo

C/ Jesús Arias de Velasco s/n. 33005, Oviedo, Spain. García-Moreno E-mail: garciaolga@uniovi.es Fax. +34 985 10 31 03

<sup>2</sup>Centro de Investigación en Nanomateriales y Nanotecnología (CINN) – Consejo Superior de Investigaciones Científicas (CSIC)
Universidad de Oviedo (UO)

Avda. de la Vega, 4-6, 33940 El Entrego, Asturias, Spain

<sup>3</sup>Leibniz Universität Hannover, Institut für Mineralogie

Callinstraat 3, D-30167 Hannover, Germany

<sup>4</sup>Departmento de Geociencias, Universidad de Los Andes

Carrera 1 # 18A-1, Bogotá, Colombia

<sup>5</sup>Departmento de Ciencias de la Tierra. Facultad de Ciencias Experimentales, Universidad de Huelva

Campus del Carmen, 21071 Huelva, Spain

#### $\dashv$ ABSTRACT $\models$

Experimental investigations and thermodynamic calculations of the phase relations of a cordierite-rich monzogranite from the Cabeza de Araya batholith (Cáceres, Spain) have been performed to understand the formation of cordierite. The experiments failed to crystallize cordierite in the pressure range 200-600MPa, in the temperature range 700-975°C and for different water activities (melt water contents between 2 and 6 wt.%). In contrast, clinopyroxene and orthopyroxene (absent in the natural mineral rock assemblage), together with biotite, were observed as ferromagnesian assemblage in a wide range of experimental conditions. Thermodynamic calculations, using the software PERPLE\_X, describe the formation of cordierite only at 200 and 400MPa and very low water contents, and the amount of cordierite formed in the models is always below 3.5 vol.%. The results indicate that cordierite is not in equilibrium with the bulk rock compositions. The most probable explanation was that cordierite nucleated and crystallized from a melt that is not in equilibrium with part of the mineral assemblage present in the magma. This "non-reactive" mineral assemblage was mainly composed of plagioclase. The silicate melts from which cordierite crystallized was more Al-rich and K-rich than the silicate melt composition in equilibrium with the bulk composition. One possible process for the high Al content of the silicate melt is related to assimilation and partial melting of Al-rich metasediments. An exo-perictetic reaction is assumed to account for both textural and geochemical observations. On the other hand, hybridization processes typical for calc-alkaline series can also explain the high proportions of "non-reactive" minerals observed in relatively high temperature magmas. This study clearly demonstrates that silicate melts in a crystal mush can depart significantly from the composition of melt that should be in equilibrium with the bulk solid assemblage.

**KEYWORDS** 

Cordierite. Monzogranites Experimental petrology. Peritectic. Pseudosections.

#### INTRODUCTION AND REGIONAL SETTING

The Variscan granitoids of the Iberian Peninsula can be sub-divided into two main types: a large group of peraluminous leucogranites, commonly associated with high-grade metamorphic zones, and a second group of granodiorites and monzogranites that also contain some intermediate metaluminous rocks (Oen, 1958, 1970; Schermerhorn, 1959; Capdevila, 1969; Corretgé, 1971; Capdevila et al., 1973; Martínez, 1974). The so-called "serie mixta" granites represent a third group of granitic rocks with mixed characteristics between the two-series mentioned above (Capdevila et al., 1973; Corretgé et al., 1977; Lagarde et al., 1992). "Serie mixta" granites show petrographic and geochemical characteristics that are intermediate between the former two series of granitic rocks. "Serie mixta" rocks, hereinafter SM granites, form plutons often related to younger granodioritesmonzogranites, but they can also form individual plutons similar, in some petrographic and geochemical aspects, to those formed by the peraluminous granites. "Serie mixta" rocks are mainly granites and monzogranitesgranodiorites with cordierite as the most characteristic ferromagnesian phase, a mineral that can also be present in the other two series of granitic rocks in the Iberian Massif. "Serie mixta" (hereinafter SM granites) rocks form high-level intrusive masses in different areas of the Iberian Massif, but essentially in the Central Extremadura Batholith in the Central Iberian Peninsula (Castro, 1984). Corretgé et al. (2004) described examples and characteristics of SM rocks in detail. The composition of the SM magmas is not typical of melt resulting from partial melting of a peraluminous protolith (i.e. peraluminous alkali-rich leucogranitic melt) and processes such as magma mixing or assimilation have been proposed to explain the geochemical signatures of SM magmas (e.g. Ugidos and Recio, 1993; García-Moreno et al., 2006). These processes may also be responsible for the abundant presence of cordierite (Ugidos et al., 2008). Explanations for the formation of this mineral are still controversial. Some authors support the idea of cordierite being result of direct crystallization from a silicate melt, other authors explain its formation from a peritectic reaction during magmatic cooling, and it is also interpreted as restitic or with xenocrystic origin (e.g. Clarke, 1995; Ugidos et al., 2008).

Both petrographic (Clarke, 1995) and experimental evidence (Green, 1976; Clemens and Wall, 1981; Puziewicz and Johannes, 1988; Holtz and Johannes, 1991; Vielzeuf and Montel, 1994; Castro *et al.*, 1999; Corretgé *et al.*, 2001) clearly support that cordierite can derive from the crystallization of peraluminous melt. However, in the case of the SM magmas, which are not typical peraluminous S-type rocks, the formation of cordierite

by direct crystallization from a melt may be questioned. Chemical composition of cordierite is also used to support its magmatic origin (Pereira and Bea, 1994). Speer (1981) and Schreyer *et al.* (1990) use textural descriptions of cordierite and the presence of different cations in the cordierite structure to explain its origin as magmatic.

Moreover, in typical SM granites such as the Cabeza de Araya batholith monzogranites, the idiomorphic shape of cordierite crystals and their mean chemical composition  $[(Mg_{0.4} \ Fe_{0.6})_2Al_4Si_5O_{18}]$  indicate a magmatic origin (García-Moreno, 2004), with a Mg# between 0.38 and 0.50 for the analysed Cabeza de Araya cordierites. Pereira and Bea (1994) classify this cordierite as magmatic.

Thus, with the central aim of constraining the stability of cordierite in typical SM igneous rocks, we performed thermodynamic calculations of phase equilibria and undertook a series of crystallization experiments at various pressures and water activities to test if cordierite crystallized from a silicate system similar in composition to SM magmas. The paper bears on an old problem that concerns a number of plutonic occurrences worldwide; hence, we present new interesting data with implications largely outside the regional area under study.

#### THE CABEZA DE ARAYA BATHOLITH

The classical example of SM granites containing cordierite is the Cabeza de Araya batholith (Corretgé, 1971) belonging to the Central Extremadura Batholith (Fig. 1). The Cabeza de Araya batholith covers an area of more than 1000km². The magma emplacement occurred after the main Variscan deformation phase (303±7Ma from whole rock Rb-Sr by Bea (2004); 302±7Ma from monazite U-Th-Pb, (Carracedo *et al.*, 2005). More recently, Rubio-Ordóñez *et al.* (2016) proposed ages, obtained by SHRIMP, from 308±1.5Ma to 305±2Ma for the sequence of the main facies in the batholith.

Castro (1985) related the emplacement of the Central Extremadura Batholith to a dextral shear zone of deformation phase 2. The emplacement of the magmas would be favoured by extensional fractures 45° from the shear zone of EW direction. Gravimetric (Audrain *et al.*, 1989) and structural and magnetic susceptibility studies (ASM) (Amice, 1990; Amice *et al.*, 1991; Vigneresse and Bouchez, 1997) describe the structure of the batholith in depth. It is deep-rooted, at approximately 11km depth, with two main well-localized roots, one SE and the other NW of the main body. These two root areas are related to deep feeding zones according to these authors. Vertical foliations are observed matching with these feeding zones.

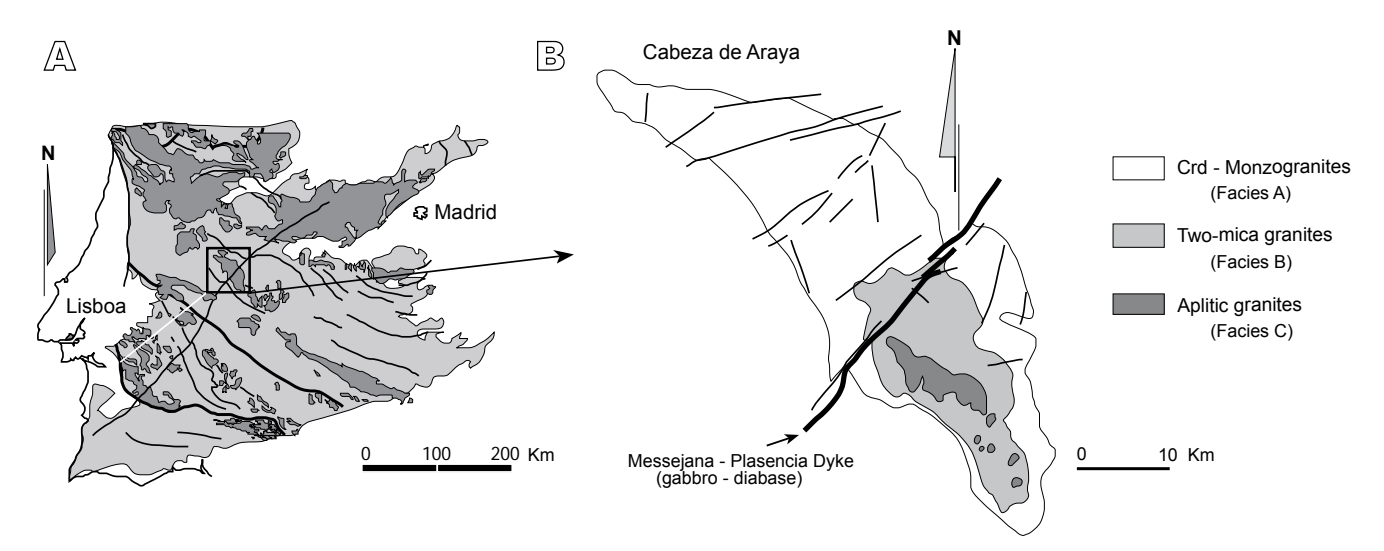


**FIGURE 1.** Cabeza de Araya map after Corretgé (1971). A) Dark gray corresponds to plutonic rocks in the Iberian Massif on the overview image on the right. B) The three main facies are distinguished for the Cabeza de Araya pluton.

The P-T conditions of formation estimated for some cordierite- and garnet-bearing Cabeza de Araya rocks are 800°C and 400±50MPa (Corretgé and Suárez, 1994). Cabeza de Araya granites show the typical zoned disposition from an external part of Crd-monzogranites-granodiorites to more leucogranitic and two-mica granites with less cordierite to the core of the pluton, and an apical aplitic leucogranitic facies compositionally identical to the peraluminous leucogranites of the Iberian Massif.

Three different main lithologies are described in the Cabeza de Araya batholith in the original work of Corretgé (1971). Table 1 summarizes the geochemical features of these main facies that are described below.

Facies A: Biotite-Muscovite-Cordierite granites and granodiorites. The characteristic of this facies is the presence of alkali feldspar megacrysts up to 10cm long and cordierite prisms (up to 4cm long). Cordierite is often pinnitized and altered to other micaceous phases. The rest of the mineral assemblage is quite uniform, with perthitic alkali feldspar, plagioclase (An<sub>20-30</sub>), quartz of different generations, abundant biotite and late blastic muscovite. Accessory minerals are andalusite, zircon and apatite with few opaque minerals. Some quartz-feldspar rich zones are spatially associated with biotite schlieren. Rapakivi texture is also described in these facies. Cordierite is found conspicuously in Facies A and more scarcely in B. The modal abundances of cordierite in Facies A is 5 vol.% (mean value) and it decreases towards the contact with Facies B. Some occasional outcrops in Facies A can show up to 250 cordierite prisms per m<sup>2</sup>, which represent more or less 15 vol.% cordierite.

Facies B: Two-mica granites, coarse-grained and non porphyritic. The mineral assemblage of these hypidiomorphic texture granites is alkali feldspar, Narich plagioclase, quartz, muscovite and biotite. Accessory minerals are zircon, apatite, andalusite, sillimanite, cordierite and tourmaline.

Facies C: Aplitic granites and leucogranites. The medium-grained mineral assemblage is similar to Facies B but with completely albitic plagioclase and a larger proportion of muscovite. Alkali feldspar is less perthitic and partially blastic.

Facies A is located in the most external zone occupying the largest area exposed in the Batholith (70%). There is a gradual transition to Facies B, to the inner zones, with a progressive decrease in the proportion of alkali feldspar megacrysts and cordierite, despite the contact between both facies can also be sharp. Facies C is intrusive in the two previous facies and is located in the central and apical zones of the Batholith. Based on the major and trace elements geochemistry of these rocks, Corretgé (1985) proposed a petrogenetic model that related Facies A and B by a unique differentiation process from the same magma. Facies C could be the result of the crystallization of a different magma with distinctive geochemical characteristics and from a different source material or petrogenetic process. This model is in agreement with a multi-pulse intrusion, as inferred from the geochronology of Facies A, B and C (Rubio-Ordóñez et al., 2016). Emplacement of Facies A and B would have started at 308Ma and lasted 3Ma, whereas Faceis C would represent a distinct pulse at 305Ma.

The absence of facies B and C towards the North and northeast of the massif is notorious. It is not only lacking

**TABLE 1.** Chemical composition of the main facies of Cabeza de Araya batholith and tonalitic enclaves (MME) found in Facies A. Numbers in brackets are number of samples. The values are the mean values of those analyses

	Facies A (18)	Facies B (17)	Facies C (3)	MME (11)
SiO <sub>2</sub>	71.50	72.19	74.02	64.44
TiO <sub>2</sub>	0.34	0.22	0.15	1.13
$Al_2O_3$	15.13	14.65	14.51	15.89
FeO <sub>t</sub>	2.30	1.57	1.09	5.28
MnO	0.04	0.02	0.02	0.05
MgO	0.52	0.43	0.26	1.51
CaO	0.87	0.75	0.36	2.26
Na <sub>2</sub> O	3.35	3.60	3.86	4.49
K <sub>2</sub> O	4.58	4.61	4.11	2.40
$P_2O_5$	0.24	0.30	0.30	0.51
LOI	0.97	1.06	0.74	1.10
Total	99.76	99.32	99.77	98.91
Li	116.6	171.94	130.8	298.2
Be	5.58	6.26	2.97	4.27
Мо	7.01	8.81	6.47	
Sn	6.67	15.08	13.83	
Sc	30.75	9.60	1.83	15.31
V	20.14	14.78	11.46	83.58
Cr	43.91	17.14	29.29	30.58
Co	3.44	42.34	1.20	10.28
Ni	16.19	10.38	14.83	13.10
Cu	15.00	8.41	7.84	14.68
Zn	64.10	55.75	49.91	152.9
Ga	18.75	18.15	14.82	127.3
Rb	259.8	300.1	258.0	241.2
Sr	64.15	52.93	29.43	69.14
Υ	3.76	8.16	0.68	33.23
Zr	96.81	105.2	59.52	217.1
Nb	21.87	11.89	12.66	33.56
Cs	0.07			0.16
Ва	286.5	241.1	169.6	17.87
La	44.25	10.62	12.13	86.01
Ce	57.51	22.33	24.43	34.25
Pr	61.31			78.99
Nd	28.71	11.77	10.47	10.21
Sm	7.14	2.51	2.73	42.58
Eu	1.19	0.24	0.36	10.65
Gd	4.49	1.99	2.64	0.72
Tb	5.20			10.45
Dy	2.84	1.10	1.80	1.60
Но	3.36			8.48
Er	0.51			1.43
Tm	0.24	0.05	0.10	3.59
Yb	0.96	0.26	0.50	0.44
Lu	0.18	0.04	0.07	2.73
Hf	0.11			0.35
Ta	3.17	3.26	3.79	6.60
TI	2.23			2.08
Pb	30.39	24.87	22.43	12.95
Th	15.96	8.21		16.65
U	6.43	3.94		5.53
S	108.5	5.20		
As	3.34			16.88

in the map, but in the interpretation of the massif evolution as well (Vigneresse and Bouchez, 1997). This could indicate a pronounced horizontal flattening, suggesting the underlying position of Facies B, which would push up the overlying Facies A. This also points to mixing of both magmas, the more mafic Facies A (Bt-dominant) with the more felsic Facies B (Bt + Mus). This could give place to interaction out of equilibrium and to cordierite formation.

Microgranular magmatic enclaves smaller than 25cm in size occur in Facies A and with a lower occurrence in

Facies B. There are two main types according to their composition and macroscopic appearance.

Tonalitic enclaves: This type of enclaves are the most common. They have darker colour than the host, and their composition is tonalitic to granodioritic. They have hypidiomorphic fine-grained and microporphyric texture. Plagioclase in the tonalitic enclaves is more Ca-rich  $(An_{20.45})$  than the plagioclase of the host granite. Biotite is widespread with a slightly higher Mg concentration than that of the biotite of the host granite. Cordierite can be an accessory mineral. Apatite is a relatively abundant accessory mineral, together with ilmenite and zircon.

Felsic enclaves: less abundant, these are monzogranites and leucocratic granodiorites with biotite ± muscovite. They differ from the host rock by their finegrained texture. Plagioclase composition is more Na-rich or similar to the plagioclase of the host rock.

#### Petrography of cordierite from the Cabeza de Araya batholith and hypothesis for the processes related to its formation

Given that cordierite is the main phase under study, a detailed description of its petrography is exposed in this section. Cordierite occurs as prismatic crystals several cm in length and is more abundant at the margins of the batholith in Facies A, in contact with the host rock. Cordierite distribution in local domains has been previously related to bulk assimilation of pelitic material (García-Moreno et al., 2007; Díaz-Alvarado et al., 2011). Textural evidences observed in Facies A support this hypothesis. Cordierite precipitation is often constrained to local domains around pelitic xenoliths, even occurring as crystals in synneusis (Fig. 2A). Cordierite prismatic crystals are surrounded by biotite, which remains as relic from wall rock assimilation (Fig. 2B). Textural analysis shows that cordierite prisms mimic a previous foliation (Fig. 2B). The parallel orientation of biotite relics supports the xenolithic carachter of biotite. This biotite is the reactive phase that gives rise to cordierite by an exo-peritectic reaction (Fig. 2B). This exo-peritectic reaction occurred when the granite was already emplaced and partially crystallized as deduced from the textural relations with the other phases. Cordierite would crystallize accompanied by the assimilation process and associated fluid release occurring at the marginal facies. In other cases, cordierite is found as prismatic crystals and its relation with relic phases is not so clear. According to this hypothesis, we designed an experimental strategy to test the hypothesis of cordierite in equilibrium with the bulk composition of the Cabeza de Araya batholith.

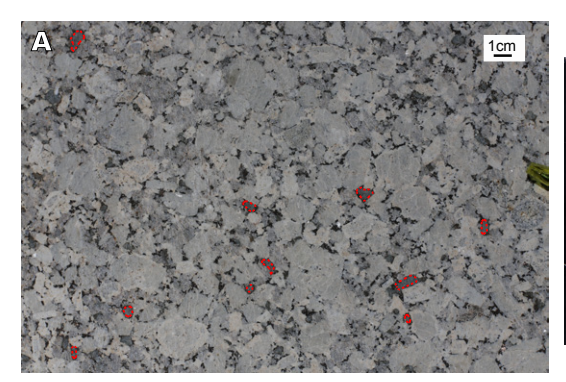
Several studies proposed that bulk assimilation processes of Al-rich metasediments by magmatic bodies explain the presence of cordierite in cordierite-rich monzogranites-granodiorites from the Iberian Peninsula (e.g. Castro et al., 1999; Ugidos et al., 2008; Díaz-Alvarado et al., 2011). This contamination process was demonstrated by isotopic studies (Ugidos et al., 2008), by the presence of zircon in the monzogranites-granodiorites which may be inherited from the surrounding pelites and by the geochemical trend of the cordierite monzogranitesgranodiorites which clearly depart from the expected evolution of cotectic melts (Díaz-Alvarado et al., 2011). This process involves mixing of silicate melts (melt from the magmatic intrusion and melt formed by partial melting of the assimilated rocks) as well as mingling processes (mechanical mixing of minerals from the assimilated bodies). Assuming such an assimilation process, only part of the mineral assemblage may be in equilibrium with the silicate melt and the composition of the silicate melt may change significantly as a function of the proportion of assimilated materials. Thus, locally cordierite may become a stable phase, although it may not be in equilibrium with the bulk magmatic composition, becoming an exo-peritectic phase.

#### **EXPERIMENTAL APPROACH**

#### Strategy and starting materials

The composition of the starting material was chosen among the most characteristic compositions of SM monzogranites-granodiorites (Facies A). This composition contains the mean value of cordierite in the batholith (~5% modal, Table 2). We synthesized glasses to reproduce the composition of a cordierite-bearing peraluminous monzogranite with the highest CaO, FeO and MgO content of the Cabeza de Araya

monzogranites (GC28069603, Table 2). We synthesized a dry glass at 1500°C from oxides and silicates (to avoid K and Na volatilization) mixtures. The homogeneity of the glass was tested with SEM images. We used this glass as the starting material for experiments at 400 and 600MPa. The materials placed in the capsules for high pressure experiments were composed by the dry glass (recalculated Al) and by various amounts of Al(OH)<sub>3</sub>. We used this method to control the amount of water added to the dry starting glass (Schmidt, 1996), as adding distilled water to the capsules sometimes led to loss of water during welding. In order to evaluate the influence of water content on cordierite stability, capsules containing nominally 2, 4 and 6 wt.% H<sub>2</sub>O were prepared. The experiments at 400 and 600MPa consisted of two-step. First, the starting assemblage was held at 975°C for 24h in order to re-homogenize the melt at this initial temperature. The temperature was then decreased isobarically to the desired temperature at a rate of 120K/h. Temperature was then held constant for a time interval between 48 and 96 hours depending on water content and temperature of each experiment (Table 3). This crystallization procedure was similar to that described by Tsuchiyama (1983, 1985) for the investigation of phase relations in magmatic systems (see also Castro et al., 1999). The composition of the glasses obtained at 975°C (after the first step) is shown in Table 2. Compositions departed slightly from the chosen natural composition, in particular for FeO and MgO. This depart is due to the crystallization of minor amounts of mafic phases. A few mineral phases, always below 5 vol.% were identified after the first homogenization step. Clinopyroxene was the most abundant phase. Mass balance calculations showed that a maximum amount of 3.5 vol.% clinopyroxene may explain the lower FeO and MgO contents of the glasses in this step. In addition, small amounts of an Al silicate (maximum 0.5 vol.%) were observed, which may result from the addition of Al(OH)<sub>3</sub> that may not be completely dissolved in the melt.



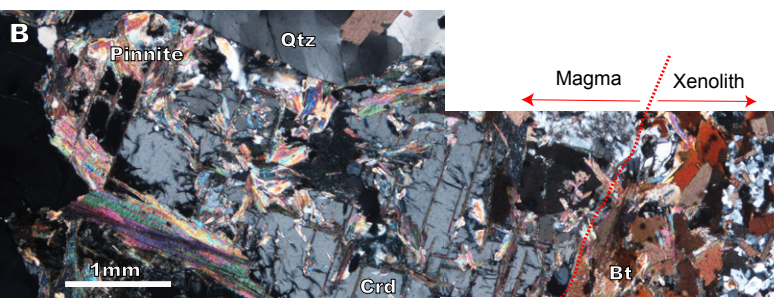


**FIGURE 2.** A) Mesoscopic aspect of the Cabeza de Araya monzogranite (Facies A) showing the large cordierite crystals with euhedral prismatic shape, occupying the interstices between the large K-feldspar crystals (red dashed areas). Cordierite prisms are pinnitized (dark green color) and surrounded by biotite remnants from xenolith assimilation. B) Photomicrograph showing cordierite growth starting from the xenolith. The red dashed line. B) indicates the magma-xenolith boundary.

**TABLE 2.** Composition of synthetic glasses used as starting material and composition of the Cabeza de Araya cordierite monzogranites

		Glasses		Crd-Monzogranite				
(wt. %)	VSCA2(a)	VSCA4(a)	VSCA6(a)	GC28069603	Modal proportio (vol.%)			
SiO <sub>2</sub>	73.65	73.10	72.99	70.87	Qtz	30.11		
TiO <sub>2</sub>	0.49	0.48	0.51	0.43	Ab	27.4		
$Al_2O_3$	14.44	14.65	14.93	14.17	Kfs	27.85		
FeO,	1.39	1.16	0.59	2.70	Bt	7.81		
MnO	0	0	0	0.02	Crd	5.33		
MgO	0.13	0.30	0.04	0.61	Ap	0.46		
CaO	1.02	0.84	0.67	1.13				
Na <sub>2</sub> O	4.23	4.78	5.29	3.55				
K₂O	4.65	4.68	4.98	4.59				
$P_2O_5$	0	0	0	0.38				
LOI	-	-	-	0.52				
Total	100.00	100.00	100.00	98.97				

a) Recast to sum 100. b) Calculated by point counting

Starting materials in experiments at 200MPa were powders of pre-hydrated glasses. The glass synthesized at 1500°C and 1atm was used to re-synthesize hydrated glasses at high pressure (500MPa) and temperature (~1200°C) using an internally heated pressure vessel (IHPV). Large AuPd capsules were placed in the IHPV that contained the dry starting glasses (see above) and the desired amount of water. The water content of the hydrated glasses was analysed using Karl-Fischer-Titration (KFT) analysis and the concentrations were within  $\pm 0.2$  wt.% H<sub>2</sub>O of the expected values: 2, 4, 6 wt.% H<sub>2</sub>O (the error of the determination is ±0.15 wt.% H<sub>2</sub>O; (Holtz et al., 1995)). The pre-hydrated glasses were then powdered, sealed in Au capsules (10-20mg), and placed in cold-seal pressure vessels (CSPV). These crystallization experiments were performed in one step and the capsules were directly brought to the desired temperature, considering that we used pre-homogenized glasses at high temperature. The run duration was between 192 and 720 hours, depending on the crystallization temperature (Table 3).

Some experiments at 200MPa were also performed (not shown in Table 3) using a fluid phase composed of mixtures of H<sub>2</sub>O and CO<sub>2</sub>, added as pure water and silver oxalate, respectively. In these experiments, water activity was mainly controlled by the proportions of CO<sub>2</sub> and H<sub>2</sub>O (*e.g.* Klimm *et al.*, 2003). The abscence of water vapour coming out of the gold capsule (determined after the experiments from weight loss after perforation) evidences that our experimental runs were water-undersaturated and fluid-absent.

The starting materials of all the runs at 400 and 600MPa and of two experiments at 200MPa contained small seeds of natural cordierite and garnet crystals (Table 3), with the purpose of favouring cordierite nucleation. With the same purpose, plagioclase seeds were added to some starting materials at 200MPa. Cordierite from Cabeza de Araya granitoids is mostly pinnitized. For this reason, seeds from a volcanic rock from Cerro del Hoyazo (Almería, Spain) (Zeck, 1992), from which we could easily select pristine crystals, were chosen. The percentage of added seeds was always below 1 wt.%.

#### **Experimental apparatus**

Experiments at 400 and 600MPa were carried out in end-loaded, solid-media piston-cylinder apparati at the University of Huelva (Spain). NaCl-graphite and CaF<sub>2</sub>-graphite cell assemblies with 12.7mm (0.5inch) diameter were used for experiments at 600 and 400MPa, respectively. Gold capsules (2.4mm inner diameter with 0.3mm wall thickness) containing approximately 10mg starting material were stored in a drying oven overnight at 120°C to overcome as much as possible adsorbed water on the glass powder and then welded shut. Oxygen fugacity in graphite-based cell assemblies was limited to a fO<sub>2</sub> interval in the range QFM to QFM-2 (Patiño Douce and Beard, 1994, 1995). These redox conditions were close to those that prevailed in the rocks of the Cabeza de Araya batholith, containing ilmenite and magnetite (Takahashi et al., 1980). Temperature was measured with Pt100-Pt87Rh13 thermocouples. Temperature stability was ±5°C during all the experimental runs. Pressure fluctuations were manually corrected and the estimated error was 50MPa.

Experiments at 200MPa were performed in horizontally oriented CSPV at Leibniz University of Hannover (Germany). The IHPV used to obtain the pre-hydrated glasses at 500MPa was also a facility of this University. The CSPV are made of Ni-rich alloy and pressurized with water. Temperature were continuously recorded by external K-type thermocouples and were within ±10°C. Experiments were quenched by removing the vessels from the furnace. The cooling rate was increased by blowing compressed air around the vessel with isobaric cooling, resulting in a quench rate of ca. 250°C/min. Redox conditions were close to the Ni-NiO buffer (Klimm et al., 2003), which are slightly more oxidizing conditions compared with the fO<sub>2</sub> conditions in the PC experiments. Cordierite is a Fe-Mg bearing phase and thus its stability may be also influenced by  $fO_2$  as it has been discussed previously (Hensen, 1986). Also, the water activity influences the  $fO_2$ , which decreases with decreasing  $H_2O$  (e.g. Botcharnikov et al., 2005), and in addition it varies with temperature, so that the exact  $fO_2$ has not been determined for each experiment. Nevertheless, we consider that the redox conditions are representative of the ones that prevailed in the formation of these rocks in nature. A further discussion on the role of oxygen fugacity conditions can be found in the thermodynamic calculations section.

#### Analytical techniques

Glasses (quenched melt) and crystalline phases were analysed using LINK-ISIS energy-dispersive spectrometer equipped on a scanning electron microscope (JEOL-JSM5410) at the University of Huelva. Na loss was corrected for glass composition measurements (López *et* 

**TABLE 3.** Summarized results of crystallization experiments

(GPa)	T (°C)	wt. % H <sub>2</sub> O (added)	Duration (hours)	Major phases	Accesory phases
Cabeza	a de Araya hy	drous sym	thetic glass	with Al(OH)₃ homogenised at 1200 °C and 0.5 GPa	
0.2	700	2	720	Qtz, Anorthoclase-Sa, Bt (0.39), Hbl? (0.39)	Ilm,Ttr
0.2	700	4	720	Qtz, Anorthoclase-Sa, Bt (0.39), Hbl? (0.34)	lln
0.2	700	6	720	Qtz, Oligoclase, Anorthoclase, Bt (0.41), Hbl?	Ilm
0.2	750	2	336	Qtz, Anorthoclase-Sa, Bt (0.47), Fs (0.40), Hbl?	IIn
0.2	750	4	360	Anorthoclase, Oligoclase, Fs-Pgt (0.42), Bt	
				(0.47)	lln
0.2	750	6	336	Oligoclase, Bt (0.46)	IIr 
0.2	800	2	192	(Qtz), Anorthoclase-Sa, Fa (0.44), Bt (0.53)	llr
0.2	800	4	192	Oligoclase, Anorthoclase, Fa (0.45)-Pgt (0.43), Bt (0.52)	lin
0.2	800	6	192	Bt (0.54), En (0.53)	llr
0.2	850	2	192	Anorthoclase-Sa, (Oligoclase), Fs (0.49), Bt (?)	IIn
0.2	850		192	En (0.59)	llr
0.2	850	6	192	Bt (0.64)	llr
Cabeza	a de Araya hy	drous syn	thetic glass	with Al(OH) $_3$ , homogenised at 1200 $^{\circ}$ C and 0.5 GPa (	d)
0.2	750	4	336	Anorthoclase, Labradorite (reacción Crd), Bt (0.46), Fs (0.39), relict Crd (0.43)	llr
Cabeza	a de Araya hy	drous synt	thetic glass	with Al(OH) <sub>3</sub> , homogenised at 1200 °C and 0.5 GPa (	dd)
0.2	750	4	336	Anorthoclase, Oligoclase, Labradorite (reaction	 Ilr
0.2	750	<b>-</b>		rim), Qtz, Fs (0.39), Bt (0.48), relict Crd (0.42)	
Cabeza	a de Araya hy	drous synt	thetic glass	with Al(OH)₃ (d)	
0.4	975→700	2	64	Aug (0.58), Spl, Sa-Anortoclase, Qtz, (Bt), (Grt) Aug-Pgt (0.77), En (0.74), Sa, Bt (0.75) (Qtz,	AI S
0.4	975 <del>→</del> 700	4	67	Oligoclase)	llr
0.4	975→750	2	72.5	Aug (0.42), Spl, Sa, Oligoclase-Andesine, Qtz	AI S
				Aug-Pgt (0.76), En (0.62), Anortoclase-Sa, Bt	
0.4	975→750	4	72.5		
0.4	975→750 975→800	4 2	72.5 70	(?), Qtz Aug-Pgt (0.41), Spl, Sa, Oligoclase-Andesine,	AI S
0.4	975→800	2	70	(?), Qtz Aug-Pgt (0.41), Spl, Sa, Oligoclase-Andesine, Qtz, Grt (0.14)	AI S
0.4	975→800 975→800	2 4	70 70	(?), Qtz Aug-Pgt (0.41), Spl, Sa, Oligoclase-Andesine, Qtz, Grt (0.14) Aug-Pgt (0.64), Anortoclase-Sa, Bt (0.55), Qtz	
0.4 0.4 0.4	975→800 975→800 975→850	2 4 4	70 70 72	(?), Qtz Aug-Pgt (0.41), Spl, Sa, Oligoclase-Andesine, Qtz, Grt (0.14) Aug-Pgt (0.64), Anortoclase-Sa, Bt (0.55), Qtz Aug (0.42), Spl, Anortoclase-Sa, Qtz	AI S
0.4 0.4 0.4 0.4	975→800 975→800 975→850 975→900	2 4 4 4	70 70 72 48	(?), Qtz Aug-Pgt (0.41), Spl, Sa, Oligoclase-Andesine, Qtz, Grt (0.14) Aug-Pgt (0.64), Anortoclase-Sa, Bt (0.55), Qtz Aug (0.42), Spl, Anortoclase-Sa, Qtz Aug (0.40), Spl, Anortoclase-Sa, Qtz, Grt?(0.0)	AI S
0.4 0.4 0.4	975→800 975→800 975→850	2 4 4	70 70 72	(?), Qtz Aug-Pgt (0.41), Spl, Sa, Oligoclase-Andesine, Qtz, Grt (0.14) Aug-Pgt (0.64), Anortoclase-Sa, Bt (0.55), Qtz Aug (0.42), Spl, Anortoclase-Sa, Qtz Aug (0.40), Spl, Anortoclase-Sa, Qtz, Grt?(0.0) Aug(0.48), Fs(0.49), (Andesine)	AI S
0.4 0.4 0.4 0.4	975→800 975→800 975→850 975→900	2 4 4 4	70 70 72 48	(?), Qtz Aug-Pgt (0.41), Spl, Sa, Oligoclase-Andesine, Qtz, Grt (0.14) Aug-Pgt (0.64), Anortoclase-Sa, Bt (0.55), Qtz Aug (0.42), Spl, Anortoclase-Sa, Qtz Aug (0.40), Spl, Anortoclase-Sa, Qtz, Grt?(0.0)	AI S AI S
0.4 0.4 0.4 0.4 0.4	975→800 975→800 975→850 975→900 975	2 4 4 4 4	70 70 72 48 24	(?), Qtz Aug-Pgt (0.41), Spl, Sa, Oligoclase-Andesine, Qtz, Grt (0.14) Aug-Pgt (0.64), Anortoclase-Sa, Bt (0.55), Qtz Aug (0.42), Spl, Anortoclase-Sa, Qtz Aug (0.40), Spl, Anortoclase-Sa, Qtz, Grt?(0.0) Aug(0.48), Fs(0.49), (Andesine)  Aug (0.65), Spl, Anortoclase-Sa, Oligoclase, Bt (0.48), Qtz Aug-Pgt (0.80), Sa, (Bt** (0.68)), (Qtz?)	AI S
0.4 0.4 0.4 0.4 0.4	975→800 975→800 975→850 975→900 975 975→700	2 4 4 4 4 2	70 70 72 48 24 70.5	(?), Qtz Aug-Pgt (0.41), Spl, Sa, Oligoclase-Andesine, Qtz, Grt (0.14) Aug-Pgt (0.64), Anortoclase-Sa, Bt (0.55), Qtz Aug (0.42), Spl, Anortoclase-Sa, Qtz Aug (0.40), Spl, Anortoclase-Sa, Qtz, Grt?(0.0) Aug(0.48), Fs(0.49), (Andesine)  Aug (0.65), Spl, Anortoclase-Sa, Oligoclase, Bt (0.48), Qtz Aug-Pgt (0.80), Sa, (Bt** (0.68)), (Qtz?)	AI S AI S
0.4 0.4 0.4 0.4 0.4 0.6 0.6	975→800 975→800 975→850 975→900 975 975→700 975→700 975→700	2 4 4 4 4 2 4	70 70 72 48 24 70.5	(?), Qtz Aug-Pgt (0.41), Spl, Sa, Oligoclase-Andesine, Qtz, Grt (0.14) Aug-Pgt (0.64), Anortoclase-Sa, Bt (0.55), Qtz Aug (0.42), Spl, Anortoclase-Sa, Qtz Aug (0.40), Spl, Anortoclase-Sa, Qtz, Grt?(0.0) Aug(0.48), Fs(0.49), (Andesine)  Aug (0.65), Spl, Anortoclase-Sa, Oligoclase, Bt (0.48), Qtz Aug-Pgt (0.80), Sa, (Bt** (0.68)), (Qtz?) Di (0.85), Sa, (Bt** (0.78))	AI S
0.4 0.4 0.4 0.4 0.4 0.6 0.6 0.6	975→800 975→800 975→850 975→900 975 975→700 975→700 975→750	2 4 4 4 4 2 4 6 2	70 70 72 48 24 70.5 72 72 64	(?), Qtz Aug-Pgt (0.41), Spl, Sa, Oligoclase-Andesine, Qtz, Grt (0.14) Aug-Pgt (0.64), Anortoclase-Sa, Bt (0.55), Qtz Aug (0.42), Spl, Anortoclase-Sa, Qtz Aug (0.40), Spl, Anortoclase-Sa, Qtz, Grt?(0.0) Aug(0.48), Fs(0.49), (Andesine)  Aug (0.65), Spl, Anortoclase-Sa, Oligoclase, Bt (0.48), Qtz Aug-Pgt (0.80), Sa, (Bt** (0.68)), (Qtz?) Di (0.85), Sa, (Bt** (0.78)) Aug (0.51), Spl, Sa, (Bt?), Qtz	AI S AI S AI S
0.4 0.4 0.4 0.4 0.4 0.6 0.6	975→800 975→800 975→850 975→900 975 975→700 975→700 975→700	2 4 4 4 4 2 4 6	70 70 72 48 24 70.5 72 72	(?), Qtz Aug-Pgt (0.41), Spl, Sa, Oligoclase-Andesine, Qtz, Grt (0.14) Aug-Pgt (0.64), Anortoclase-Sa, Bt (0.55), Qtz Aug (0.42), Spl, Anortoclase-Sa, Qtz Aug (0.40), Spl, Anortoclase-Sa, Qtz, Grt?(0.0) Aug(0.48), Fs(0.49), (Andesine)  Aug (0.65), Spl, Anortoclase-Sa, Oligoclase, Bt (0.48), Qtz Aug-Pgt (0.80), Sa, (Bt** (0.68)), (Qtz?) Di (0.85), Sa, (Bt** (0.78)) Aug (0.51), Spl, Sa, (Bt?), Qtz Aug-Pgt (0.68), Spl, Sa-Anortoclase, Bt (?), Qtz Aug-Pgt (0.68), En (0.67), Spl, Sa-Anortoclase,	AI S AI S AI S AI Sil, II
0.4 0.4 0.4 0.4 0.6 0.6 0.6 0.6 0.6	975→800 975→800 975→850 975→900 975 975→700 975→700 975→750 975→750	2 4 4 4 4 2 4 6 2 4	70 70 72 48 24 70.5 72 72 64 64	(?), Qtz Aug-Pgt (0.41), Spl, Sa, Oligoclase-Andesine, Qtz, Grt (0.14) Aug-Pgt (0.64), Anortoclase-Sa, Bt (0.55), Qtz Aug (0.42), Spl, Anortoclase-Sa, Qtz Aug (0.40), Spl, Anortoclase-Sa, Qtz, Grt?(0.0) Aug(0.48), Fs(0.49), (Andesine)  Aug (0.65), Spl, Anortoclase-Sa, Oligoclase, Bt (0.48), Qtz Aug-Pgt (0.80), Sa, (Bt** (0.68)), (Qtz?) Di (0.85), Sa, (Bt** (0.78)) Aug (0.51), Spl, Sa, (Bt?), Qtz Aug-Pgt (0.68), En (0.67), Spl, Sa-Anortoclase, Oligoclase, Bt (0,49), (Grt (0.16)), Qtz Aug-Pgt (0.59), Spl, Sa-Anortoclase, Bt (0.7),	AI S AI S AI S AI Sil, II AI S
0.4 0.4 0.4 0.4 0.6 0.6 0.6 0.6 0.6 0.6	975→800 975→800 975→850 975→900 975 975→700 975→700 975→750 975→750 975→750	2 4 4 4 4 2 4 6 2 4 6	70 70 72 48 24 70.5 72 72 64 64 64	(?), Qtz Aug-Pgt (0.41), Spl, Sa, Oligoclase-Andesine, Qtz, Grt (0.14) Aug-Pgt (0.64), Anortoclase-Sa, Bt (0.55), Qtz Aug (0.42), Spl, Anortoclase-Sa, Qtz Aug (0.40), Spl, Anortoclase-Sa, Qtz, Grt?(0.0) Aug(0.48), Fs(0.49), (Andesine)  Aug (0.65), Spl, Anortoclase-Sa, Oligoclase, Bt (0.48), Qtz Aug-Pgt (0.80), Sa, (Bt** (0.68)), (Qtz?) Di (0.85), Sa, (Bt** (0.78)) Aug (0.51), Spl, Sa, (Bt?), Qtz Aug-Pgt (0.68), En (0.67), Spl, Sa-Anortoclase, Oligoclase, Bt (0,49), (Grt (0.16)), Qtz	AI S AI S
0.4 0.4 0.4 0.4 0.6 0.6 0.6 0.6 0.6 0.6	975→800 975→800 975→850 975→900 975 975→700 975→700 975→750 975→750 975→750 975→800	2 4 4 4 4 2 4 6 2 4 6	70 70 72 48 24 70.5 72 72 64 64 64	(?), Qtz Aug-Pgt (0.41), Spl, Sa, Oligoclase-Andesine, Qtz, Grt (0.14) Aug-Pgt (0.64), Anortoclase-Sa, Bt (0.55), Qtz Aug (0.42), Spl, Anortoclase-Sa, Qtz Aug (0.40), Spl, Anortoclase-Sa, Qtz, Grt?(0.0) Aug(0.48), Fs(0.49), (Andesine)  Aug (0.65), Spl, Anortoclase-Sa, Oligoclase, Bt (0.48), Qtz Aug-Pgt (0.80), Sa, (Bt** (0.68)), (Qtz?) Di (0.85), Sa, (Bt** (0.78)) Aug (0.51), Spl, Sa, (Bt?), Qtz Aug (0.50), Spl, Sa-Anortoclase, Bt (?), Qtz Aug-Pgt (0.68), En (0.67), Spl, Sa-Anortoclase, Oligoclase, Bt (0,49), (Grt (0.16)), Qtz Aug-Pgt (0.59), Spl, Sa-Anortoclase, Bt (0.7), Qtz	AI S AI S AI S AI Sil, III AI S AI S
0.4 0.4 0.4 0.4 0.6 0.6 0.6 0.6 0.6 0.6 0.6 0.6	975→800 975→800 975→850 975→900 975 975→700 975→700 975→750 975→750 975→750 975→800 975→800 975→800	2 4 4 4 4 2 4 6 2 4 6	70 70 72 48 24 70.5 72 72 64 64 64 74 74	(?), Qtz Aug-Pgt (0.41), Spl, Sa, Oligoclase-Andesine, Qtz, Grt (0.14) Aug-Pgt (0.64), Anortoclase-Sa, Bt (0.55), Qtz Aug (0.42), Spl, Anortoclase-Sa, Qtz Aug (0.40), Spl, Anortoclase-Sa, Qtz, Grt?(0.0) Aug(0.48), Fs(0.49), (Andesine)  Aug (0.65), Spl, Anortoclase-Sa, Oligoclase, Bt (0.48), Qtz Aug-Pgt (0.80), Sa, (Bt** (0.68)), (Qtz?) Di (0.85), Sa, (Bt** (0.78)) Aug (0.51), Spl, Sa, (Bt?), Qtz Aug-Pgt (0.68), En (0.67), Spl, Sa-Anortoclase, Oligoclase, Bt (0,49), (Grt (0.16)), Qtz Aug-Pgt (0.59), Spl, Sa-Anortoclase, Bt (0.7), Qtz Aug-Pgt (0.84), Sa-Anortoclase, Bt (0.7), Qtz Aug-Pgt (0.84), Sa-Anortoclase, Bt (0.8), Qtz Bt (0.81), Oligoclase	AI S AI S AI S AI SiI, II AI S AI SII, III
0.4 0.4 0.4 0.4 0.6 0.6 0.6 0.6 0.6 0.6 0.6	975→800 975→800 975→850 975→900 975 975→700 975→700 975→750 975→750 975→750 975→800 975→800	2 4 4 4 4 2 4 6 2 4 6	70 70 72 48 24 70.5 72 72 64 64 64 74	(?), Qtz Aug-Pgt (0.41), Spl, Sa, Oligoclase-Andesine, Qtz, Grt (0.14) Aug-Pgt (0.64), Anortoclase-Sa, Bt (0.55), Qtz Aug (0.42), Spl, Anortoclase-Sa, Qtz Aug (0.40), Spl, Anortoclase-Sa, Qtz, Grt?(0.0) Aug(0.48), Fs(0.49), (Andesine)  Aug (0.65), Spl, Anortoclase-Sa, Oligoclase, Bt (0.48), Qtz Aug-Pgt (0.80), Sa, (Bt** (0.68)), (Qtz?) Di (0.85), Sa, (Bt** (0.78)) Aug (0.51), Spl, Sa-Anortoclase, Bt (?), Qtz Aug-Pgt (0.68), En (0.67), Spl, Sa-Anortoclase, Oligoclase, Bt (0,49), (Grt (0.16)), Qtz Aug-Pgt (0.59), Spl, Sa-Anortoclase, Bt (0.7), Qtz Aug-Pgt (0.84), Sa-Anortoclase, Bt (0.8), Qtz Bt (0.81), Oligoclase Aug (0.70)-Pgt (0.50), Spl, Sa-Anortoclase, Qtz Aug-Pgt (0.78), En (0.68), (Sa-Anortoclase **), Bt	AI S AI S AI S AI SiI, II AI S AI SII, III
0.4 0.4 0.4 0.4 0.6 0.6 0.6 0.6 0.6 0.6 0.6 0.6	975→800 975→800 975→850 975→900 975 975→700 975→700 975→750 975→750 975→800 975→800 975→800 975→800 975→850 975→850	2 4 4 4 4 2 4 6 2 4 6 2 4 6 2 4 6 2 4	70 70 72 48 24 70.5 72 72 64 64 64 74 74 73 73	(?), Qtz Aug-Pgt (0.41), Spl, Sa, Oligoclase-Andesine, Qtz, Grt (0.14) Aug-Pgt (0.64), Anortoclase-Sa, Bt (0.55), Qtz Aug (0.42), Spl, Anortoclase-Sa, Qtz Aug (0.40), Spl, Anortoclase-Sa, Qtz, Grt?(0.0) Aug(0.48), Fs(0.49), (Andesine)  Aug (0.65), Spl, Anortoclase-Sa, Oligoclase, Bt (0.48), Qtz Aug-Pgt (0.80), Sa, (Bt** (0.68)), (Qtz?) Di (0.85), Sa, (Bt** (0.78)) Aug (0.51), Spl, Sa, (Bt?), Qtz Aug-Pgt (0.68), En (0.67), Spl, Sa-Anortoclase, Oligoclase, Bt (0.49), (Grt (0.16)), Qtz Aug-Pgt (0.59), Spl, Sa-Anortoclase, Bt (0.7), Qtz Aug-Pgt (0.84), Sa-Anortoclase, Bt (0.8), Qtz Bt (0.81), Oligoclase Aug (0.70)-Pgt (0.50), Spl, Sa-Anortoclase, Qtz Aug-Pgt (0.78), En (0.68), (Sa-Anortoclase **), Bt (0.73)	AI S AI S AI S AI S AI S AI S AI SiI, III
0.4 0.4 0.4 0.4 0.6 0.6 0.6 0.6 0.6 0.6 0.6 0.6	975→800 975→800 975→850 975→900 975 975→700 975→700 975→750 975→750 975→750 975→800 975→800 975→850 975→850 975→850	2 4 4 4 2 4 6 2 4 6 2 4 6 2 4 6	70 70 72 48 24 70.5 72 72 64 64 64 74 74 73 73	(?), Qtz Aug-Pgt (0.41), Spl, Sa, Oligoclase-Andesine, Qtz, Grt (0.14) Aug-Pgt (0.64), Anortoclase-Sa, Bt (0.55), Qtz Aug (0.42), Spl, Anortoclase-Sa, Qtz Aug (0.40), Spl, Anortoclase-Sa, Qtz, Grt?(0.0) Aug(0.48), Fs(0.49), (Andesine)  Aug (0.65), Spl, Anortoclase-Sa, Oligoclase, Bt (0.48), Qtz Aug-Pgt (0.80), Sa, (Bt** (0.68)), (Qtz?) Di (0.85), Sa, (Bt** (0.78)) Aug (0.51), Spl, Sa, (Bt?), Qtz Aug-Pgt (0.68), En (0.67), Spl, Sa-Anortoclase, Oligoclase, Bt (0,49), (Grt (0.16)), Qtz Aug-Pgt (0.59), Spl, Sa-Anortoclase, Bt (0.7), Qtz Aug-Pgt (0.84), Sa-Anortoclase, Bt (0.81), Oligoclase Aug (0.70)-Pgt (0.50), Spl, Sa-Anortoclase, Qtz Aug-Pgt (0.78), En (0.68), (Sa-Anortoclase **), Bt (0.73) Aug (0.89), Anortoclase	AI S AI S AI S AI S AI S AI SII, II AI SII, II
0.4 0.4 0.4 0.4 0.6 0.6 0.6 0.6 0.6 0.6 0.6 0.6	975→800 975→800 975→850 975→900 975 975→700 975→700 975→750 975→750 975→750 975→800 975→800 975→800 975→850 975→850 975→850 975→850 975→900	2 4 4 4 4 2 4 6 2 4 6 2 4 6 2 4 6 2 4 6 2 4 6 6 2 4 6 6 2 4 6 6 2 4 6 6 2 4 6 6 2 4 6 6 2 4 6 6 2 4 6 6 2 4 6 6 2 4 6 6 2 4 6 6 2 4 4 6 2 4 4 6 2 4 4 6 2 4 4 6 2 4 4 6 2 4 4 6 2 4 4 6 2 4 4 6 2 4 4 6 2 4 4 4 4	70 70 72 48 24 70.5 72 72 64 64 64 74 74 73 73 73 48	(?), Qtz Aug-Pgt (0.41), Spl, Sa, Oligoclase-Andesine, Qtz, Grt (0.14) Aug-Pgt (0.64), Anortoclase-Sa, Bt (0.55), Qtz Aug (0.42), Spl, Anortoclase-Sa, Qtz Aug (0.40), Spl, Anortoclase-Sa, Qtz, Grt?(0.0) Aug(0.48), Fs(0.49), (Andesine)  Aug (0.65), Spl, Anortoclase-Sa, Oligoclase, Bt (0.48), Qtz Aug-Pgt (0.80), Sa, (Bt** (0.68)), (Qtz?) Di (0.85), Sa, (Bt** (0.78)) Aug (0.51), Spl, Sa, (Bt?), Qtz Aug (0.50), Spl, Sa-Anortoclase, Bt (?), Qtz Aug-Pgt (0.68), En (0.67), Spl, Sa-Anortoclase, Oligoclase, Bt (0.49), (Grt (0.16)), Qtz Aug-Pgt (0.59), Spl, Sa-Anortoclase, Bt (0.7), Qtz Aug-Pgt (0.84), Sa-Anortoclase, Bt (0.8), Qtz Bt (0.81), Oligoclase Aug (0.70)-Pgt (0.50), Spl, Sa-Anortoclase, Qtz Aug-Pgt (0.78), En (0.68), (Sa-Anortoclase **), Bt (0.73) Aug (0.89), Anortoclase Aug (0.52), Spl, Anortoclase-Sa, (Grt (0.15)), Qtz Aug-Pgt (0.82), En (0.68), Spl, Anortoclase,	AI S AI S AI SiI, II AI S AI SiI, II AI SiI, II
0.4 0.4 0.4 0.4 0.6 0.6 0.6 0.6 0.6 0.6 0.6 0.6	975→800 975→800 975→850 975→900 975 975→700 975→700 975→750 975→750 975→750 975→800 975→800 975→850 975→850 975→850	2 4 4 4 2 4 6 2 4 6 2 4 6 2 4 6	70 70 72 48 24 70.5 72 72 64 64 64 74 74 73 73 73 48 48	(?), Qtz Aug-Pgt (0.41), Spl, Sa, Oligoclase-Andesine, Qtz, Grt (0.14) Aug-Pgt (0.64), Anortoclase-Sa, Bt (0.55), Qtz Aug (0.42), Spl, Anortoclase-Sa, Qtz Aug (0.40), Spl, Anortoclase-Sa, Qtz, Grt?(0.0) Aug(0.48), Fs(0.49), (Andesine)  Aug (0.65), Spl, Anortoclase-Sa, Oligoclase, Bt (0.48), Qtz Aug-Pgt (0.80), Sa, (Bt** (0.68)), (Qtz?) Di (0.85), Sa, (Bt** (0.78)) Aug (0.51), Spl, Sa, (Bt?), Qtz Aug-Pgt (0.68), En (0.67), Spl, Sa-Anortoclase, Oligoclase, Bt (0.49), (Grt (0.16)), Qtz Aug-Pgt (0.59), Spl, Sa-Anortoclase, Bt (0.7), Qtz Aug-Pgt (0.84), Sa-Anortoclase, Bt (0.7), Qtz Aug-Pgt (0.84), Sa-Anortoclase, Bt (0.8), Qtz Bt (0.81), Oligoclase Aug (0.70)-Pgt (0.50), Spl, Sa-Anortoclase, Qtz Aug-Pgt (0.78), En (0.68), (Sa-Anortoclase **), Bt (0.73) Aug (0.89), Anortoclase Aug (0.52), Spl, Anortoclase-Sa, (Grt (0.15)), Qtz Aug-Pgt (0.82), En (0.68), Spl, Anortoclase, Oligoclase	AI S AI S AI SiI, II AI S AI SiI, II AI SiI, II
0.4 0.4 0.4 0.4 0.6 0.6 0.6 0.6 0.6 0.6 0.6 0.6	975→800 975→800 975→850 975→900 975 975→700 975→700 975→750 975→750 975→750 975→800 975→800 975→800 975→850 975→850 975→850 975→850 975→900	2 4 4 4 4 2 4 6 2 4 6 2 4 6 2 4 6 2 4 6 2 4 6 6 2 4 6 6 2 4 6 6 2 4 6 6 2 4 6 6 2 4 6 6 2 4 6 6 2 4 6 6 2 4 6 6 2 4 6 6 2 4 6 6 2 4 4 6 2 4 4 6 2 4 4 6 2 4 4 6 2 4 4 6 2 4 4 6 2 4 4 6 2 4 4 6 2 4 4 6 2 4 4 4 4	70 70 72 48 24 70.5 72 72 64 64 64 74 74 73 73 73 48	(?), Qtz Aug-Pgt (0.41), Spl, Sa, Oligoclase-Andesine, Qtz, Grt (0.14) Aug-Pgt (0.64), Anortoclase-Sa, Bt (0.55), Qtz Aug (0.42), Spl, Anortoclase-Sa, Qtz Aug (0.40), Spl, Anortoclase-Sa, Qtz, Grt?(0.0) Aug(0.48), Fs(0.49), (Andesine)  Aug (0.65), Spl, Anortoclase-Sa, Oligoclase, Bt (0.48), Qtz Aug-Pgt (0.80), Sa, (Bt** (0.68)), (Qtz?) Di (0.85), Sa, (Bt** (0.78)) Aug (0.51), Spl, Sa, (Bt?), Qtz Aug (0.50), Spl, Sa-Anortoclase, Bt (?), Qtz Aug-Pgt (0.68), En (0.67), Spl, Sa-Anortoclase, Oligoclase, Bt (0.49), (Grt (0.16)), Qtz Aug-Pgt (0.59), Spl, Sa-Anortoclase, Bt (0.7), Qtz Aug-Pgt (0.84), Sa-Anortoclase, Bt (0.8), Qtz Bt (0.81), Oligoclase Aug (0.70)-Pgt (0.50), Spl, Sa-Anortoclase, Qtz Aug-Pgt (0.78), En (0.68), (Sa-Anortoclase **), Bt (0.73) Aug (0.89), Anortoclase Aug (0.52), Spl, Anortoclase-Sa, (Grt (0.15)), Qtz Aug-Pgt (0.82), En (0.68), Spl, Anortoclase,	AI S
0.4 0.4 0.4 0.4 0.6 0.6 0.6 0.6 0.6 0.6 0.6 0.6	975→800 975→800 975→850 975→900 975 975→700 975→750 975→750 975→750 975→800 975→800 975→850 975→850 975→850 975→850 975→900 975→900	2 4 4 4 2 4 6 2 4 6 2 4 6 2 4 6 2 4 6 2 4 4 4 4	70 70 72 48 24 70.5 72 72 64 64 64 74 74 73 73 73 48 48	(?), Qtz Aug-Pgt (0.41), Spl, Sa, Oligoclase-Andesine, Qtz, Grt (0.14) Aug-Pgt (0.64), Anortoclase-Sa, Bt (0.55), Qtz Aug (0.42), Spl, Anortoclase-Sa, Qtz Aug (0.40), Spl, Anortoclase-Sa, Qtz, Grt?(0.0) Aug(0.48), Fs(0.49), (Andesine)  Aug (0.65), Spl, Anortoclase-Sa, Oligoclase, Bt (0.48), Qtz Aug-Pgt (0.80), Sa, (Bt** (0.68)), (Qtz?) Di (0.85), Sa, (Bt** (0.78)) Aug (0.51), Spl, Sa, (Bt?), Qtz Aug-Pgt (0.68), En (0.67), Spl, Sa-Anortoclase, Oligoclase, Bt (0.49), (Grt (0.16)), Qtz Aug-Pgt (0.59), Spl, Sa-Anortoclase, Bt (0.7), Qtz Aug-Pgt (0.84), Sa-Anortoclase, Bt (0.7), Qtz Aug-Pgt (0.84), Sa-Anortoclase, Bt (0.8), Qtz Bt (0.81), Oligoclase Aug (0.70)-Pgt (0.50), Spl, Sa-Anortoclase, Qtz Aug-Pgt (0.78), En (0.68), (Sa-Anortoclase **), Bt (0.73) Aug (0.89), Anortoclase Aug (0.52), Spl, Anortoclase-Sa, (Grt (0.15)), Qtz Aug-Pgt (0.82), En (0.68), Spl, Anortoclase, Oligoclase	AI S AI S AI S AI SiI, II AI SiI, II AI SiI, II AI SiI, II AI SiI, II
0.4 0.4 0.4 0.4 0.6 0.6 0.6 0.6 0.6 0.6 0.6 0.6	975→800 975→800 975→850 975→900 975 975→700 975→700 975→750 975→750 975→750 975→800 975→800 975→850 975→850 975→850 975→850 975→900 975→900	2 4 4 4 2 4 6 2 4 6 2 4 6 2 4 6 2 4 6 2 4 6 6 2 4 6 6 2 4 6 6 2 4 6 6 2 4 6 6 2 4 6 6 2 4 6 6 6 2 4 6 6 6 2 4 6 6 6 2 4 6 6 6 2 4 6 6 6 2 4 6 6 2 4 6 6 2 4 6 6 2 4 6 6 2 4 6 6 2 4 6 6 2 4 6 6 2 4 6 6 2 4 6 6 2 4 6 6 2 4 6 6 2 4 6 6 2 4 6 6 2 4 6 6 2 4 6 6 2 4 4 6 2 4 4 6 2 4 6 2 4 6 2 4 6 2 4 6 4 6	70 70 72 48 24 70.5 72 72 64 64 64 74 74 73 73 73 48 48	(?), Qtz Aug-Pgt (0.41), Spl, Sa, Oligoclase-Andesine, Qtz, Grt (0.14) Aug-Pgt (0.64), Anortoclase-Sa, Bt (0.55), Qtz Aug (0.42), Spl, Anortoclase-Sa, Qtz Aug (0.40), Spl, Anortoclase-Sa, Qtz, Grt?(0.0) Aug(0.48), Fs(0.49), (Andesine)  Aug (0.65), Spl, Anortoclase-Sa, Oligoclase, Bt (0.48), Qtz Aug-Pgt (0.80), Sa, (Bt** (0.68)), (Qtz?) Di (0.85), Sa, (Bt** (0.78)) Aug (0.51), Spl, Sa, (Bt?), Qtz Aug (0.50), Spl, Sa-Anortoclase, Bt (?), Qtz Aug-Pgt (0.68), En (0.67), Spl, Sa-Anortoclase, Oligoclase, Bt (0.49), (Grt (0.16)), Qtz Aug-Pgt (0.59), Spl, Sa-Anortoclase, Bt (0.7), Qtz Aug-Pgt (0.84), Sa-Anortoclase, Bt (0.8), Qtz Bt (0.81), Oligoclase Aug (0.70)-Pgt (0.50), Spl, Sa-Anortoclase, Qtz Aug-Pgt (0.78), En (0.68), (Sa-Anortoclase **), Bt (0.73) Aug (0.89), Anortoclase Aug (0.52), Spl, Anortoclase-Sa, (Grt (0.15)), Qtz Aug-Pgt (0.82), En (0.68), Spl, Anortoclase, Oligoclase Aug (0.56), Spl, Anortoclase, (Qtz?)	AI S AI S AI S AI SiI, III AI S AI S

Numbers in brackets are #Mg for ferromagnesian minerals. Symbols after Kretz (1983). Hbl unclassified amphibol? identified phase with uncertain composition; \*\* interpreted phase not clearly identified; experiments denoted with (d) are doped with Crd and Grt seeds, and (dd) are doped with Crd, Grt and Pl seeds.

al., 2005). Some experimental products were analyzed with an electron microprobe Camebax SX100 at the Leibniz University of Hannover. Crystalline phases were analysed with 15kV acceleration voltage, 10nA sample current and 10s total counting time. To minimise the migration of alkalis during glass analysis the analytical conditions were set to 15kV, 6nA and 5s total counting time and the beam was defocused up to 20 $\mu$ m when possible (lowest value was 5 $\mu$ m), and Na was measured first.

#### **Experimental results**

Table 3 summarizes the experimental results obtained at 200, 400 and 600MPa and at a temperature range between 700 and 975°C. Unfortunately, the size of the crystallized phases in almost all the runs were too small to have a complete set of data on the geochemical characterization of the different phases for all the tested conditions. Nevertheless, Table 3 shows the Mg# [Mg#=Mg/(Fe<sub>tot</sub>+Mg) molar] of the ferromagnesian phases and the An content in plagioclase when we could obtain proper analyses.

We start the description of the mineral phases present in the experimental samples with the ferromagnesian phases as they are distinctive of each conditions (whereas quartz and feldspar where ubiquitous at proper experimental conditions).

Initially, we performed experiments at 600MPa and 700°C with three different water contents without adding any mineral seeds. In these experiments, the main ferromagnesian mineral phase was clinopyroxene. This mineral phase has never been described in SM granites. Because cordierite is the most characteristic mafic phase in the natural assemblage, and because garnet may also be stable at high pressure in such composition, seeds of cordierite and garnet were added to the starting material to avoid possible nucleation problems for these phases. The experimental results were similar and clinopyroxene was the main ferromagnesian phase in all doped experiments at 400 and 600MPa, whereas biotite occurred mainly at 200MPa (Table 3).

Clinopyroxene crystals have a size of approximately 10µm and euhedral shape, especially at high temperature and high water activity (Fig. 3A). Clinopyroxene shows complex cores with resorption texture, so that accurate microprobe analyses were not possible even in large crystals. Crystallization of clinopyroxene in the first step of the 400 and 600MPa runs was probably the cause of this texture. This high temperature clinopyroxene reacted with the melt in the second step, leading to intricate texture. However, the rims of the crystals did not show resorption texture and the external shapes were euhedral, indicating

that the clinopyroxene rims were in equilibrium with the melt. Clinopyroxene was only observed at 400 and 600MPa. Orthopyroxene was observed in some runs at 200 and 600MPa. At 200MPa, Mg# of clinopyroxene increased with temperature.

Biotite crystals are small and typically exposed as fine needles, making it difficult to obtain accurate analyses. However, the Mg# (Table 3) could be used as an indication for the compositional range of biotite. Most runs at 850°C and below contained biotite. At 200MPa, Mg# increases with temperature. The Mg# of biotites obtained at 400 and 600MPa is more difficult to discuss because of the lack of systematic data, but Mg# seems to be higher at higher pressure. In addition,  $fO_2$  could have an effect on the Mg# ratio of biotite in both types of experiments (cold- seal and piston-cylinder).

Spinel occurred in a wide range of experiments at 400 and 600MPa and appeared mainly as aggregates with other small mineral phases (impossible to discriminate with the analytical techniques used in this study; see Fig. 3B). Mass balance calculations using bulk analysis of these aggregates indicate a composition of a possible mixture of 75% hercynite (Mg#=20-55) and 25% plagioclase (~An<sub>30</sub>). These "spinel like" aggregates in the core of feldspar crystals might be phases already present in the first experimental step at high temperature. The presence of these relict phases could be explained by the reaction of Al(OH)<sub>3</sub> (added as source of water) with the surrounding melt in early stages of the experiment. Figure 4 shows the topological plot of these "spinel like" aggregates in the triangle defined by theoretical pure hercynite, spinel and plagioclase compositions. The composition of the aggregates corresponds to a mixture of plagioclase and spinel with an intermediate composition between hercynite and spinel. In the same way as spinel, aluminium silicates needles (composition close to that of mullite) generally associated with quartz were included in feldspar cores and might be remnants of products from the first high temperature step. The presence of mullite crystals in runs containing 2 and 4 wt.% H<sub>2</sub>O could be a result of local high alumina activities after the dehydration of Al(OH)<sub>3</sub> during the first step. In any case, considering the very low amount of this relict assemblage, the reactive composition is not expected to be modified significantly (Pichavant, et al., 2007) and the phase assemblage observed in the experimental products are considered to be representative of equilibrium phase assemblages for the starting composition.

Garnet was present only in small volumetric proportions (<1 vol.%) as undissolved relict "seeds" added to the hydrous glasses in some experiments. It consists of small crystals of almandine (Mg#=0.15) with the same

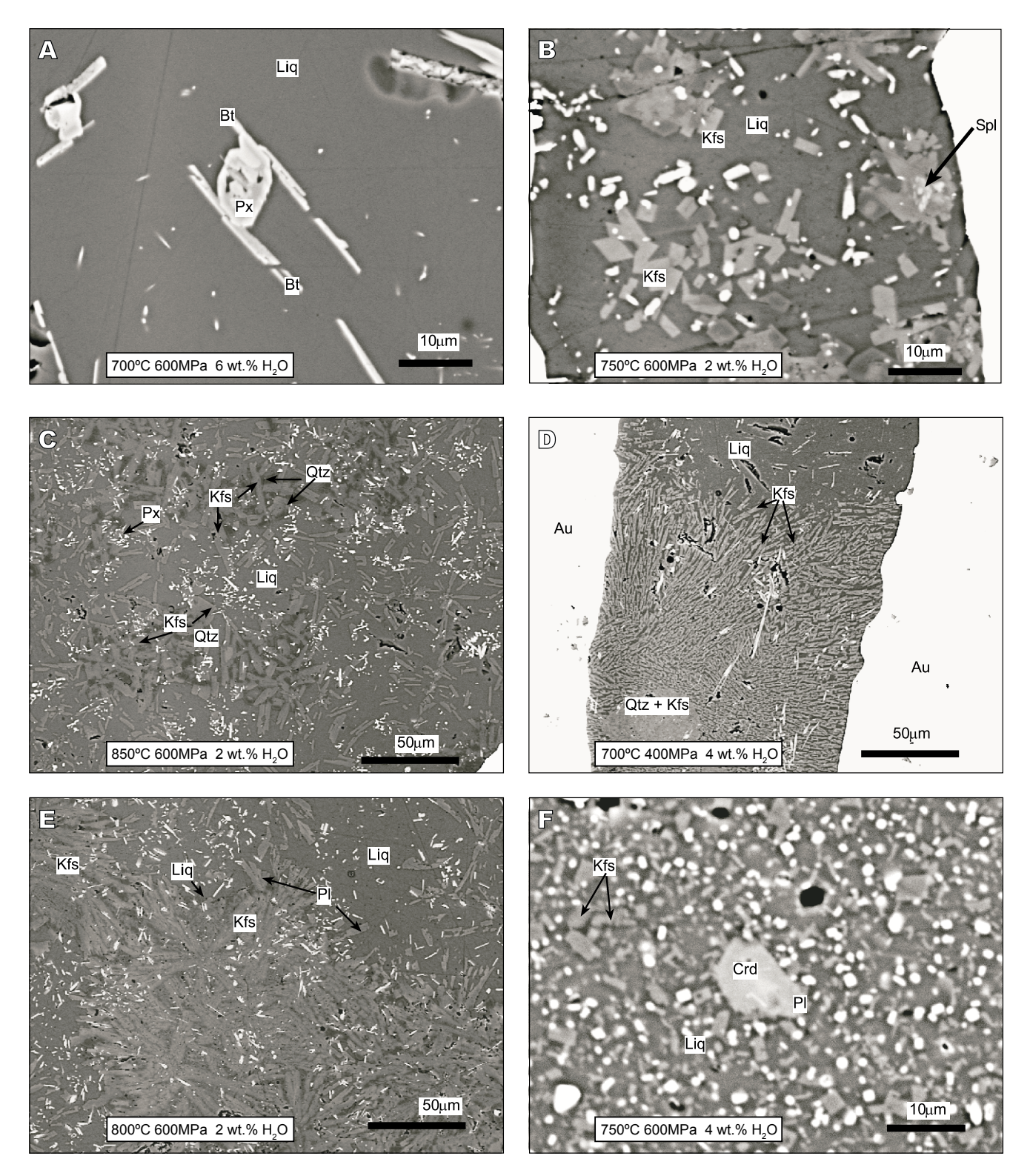


**FIGURE 3.** SEM images of some experimental products: A) 700°C, 600MPa and 6 wt.% initial water; B) 750°C, 600MPa and 2 wt.% initial water; C) 850°C, 600MPa and 2 wt.% initial water; D) 700°C, 400MPa and 4 wt.% initial water; E) 800°C, 600MPa and 2 wt.% initial water; F) 750°C, 200MPa and 4 wt.% initial water.

composition as the seeds added to the glasses. Amphibole was present only at 200MPa at 700 and 750°C. The crystals

had very small sizes  $(2\mu m)$  and could only be analysed qualitatively.

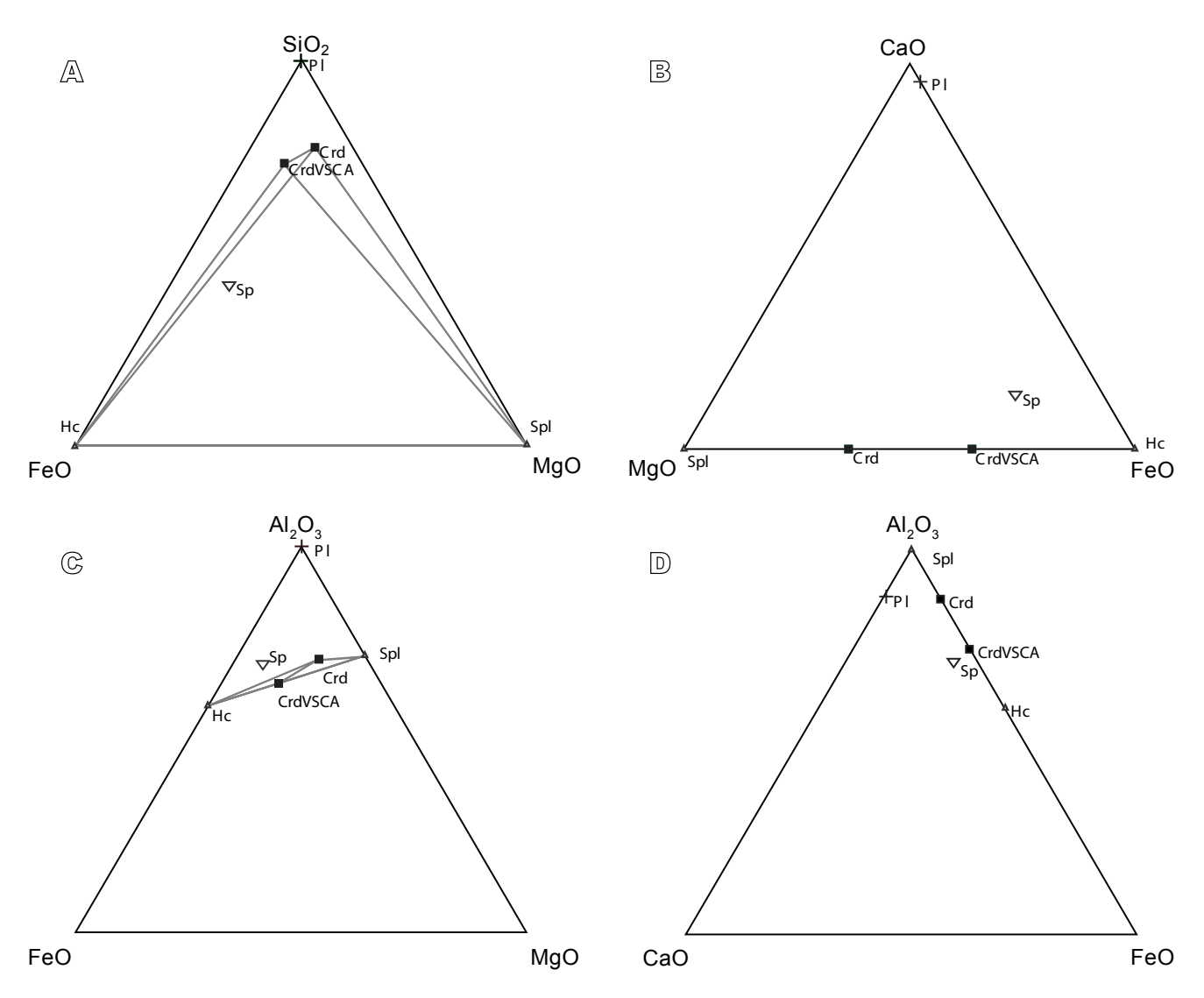


**FIGURE 4.** Topological plot of "spinel like" aggregates found in the experiments in the systems: A) FeO-SiO<sub>2</sub>-MgO; B) MgO-CaO<sub>2</sub>-FeO; C) FeO-Al<sub>2</sub>O<sub>3</sub>-MgO; D) CaO- Al<sub>2</sub>O<sub>3</sub>-FeO.

Quartz was observed in experiments with low melt fractions (either low water activity, low temperature or both). Quartz was in some cases spatially associated with feldspar and symplectite-like texture of quartz and feldspar could be observed (Fig. 3C). Isolated quartz crystals were typically round and irregular. Quartz crystals could also form aggregates of round crystals.

Feldspars were the most abundant phases (together with Cpx) in our experiments. They were present in the whole pressure range from the lowest temperature almost to the liquidus for all initial water contents. The morphology of feldspars depends upon the water content of the melt from which they crystallized (and consequently on the degree of undercooling). In the experiments with initially low water contents (and at low temperature), feldspars typically crystallized in aggregates of crystals forming spherulites

composed of thin needle-like crystals. In experiments with higher initial water contents, crystals were individualized and with *ca.* 15µm. However, the formation of spherulites was also probably related to the experimental approach. Spherulitic texture occurred only in the 400 and 600MPa experiments (starting from 975°C and with a second step at lower temperature) but were not identified in experiments brought directly from room temperature to the target temperature (experiments at 200MPa). Another common feature of feldspar crystallization was heterogeneous nucleation on the walls of the gold capsule or from Al-rich nuclei (spinel or Al-silicates).

Alkali feldspar was dominant over plagioclase, the latter with compositions poor in anorthitic component. Compositional differences between both kinds of feldspar were not pronounced and they could not be distinguished in BSE images because of their similar gray colour (Fig. 3E). They were difficult to distinguish even applying different contrast and brightness conditions. However, zoning could be found in some large crystals. Plagioclase had normal zoning, but it was more common to find patchy zoning in any kind of large feldspar. The most Ca-rich compositions of feldspar in our experiments were always crystal cores in contact with spinel clusters. Several large feldspar crystals exhibited inclusions of other phases such as spinel and Al-silicates mentioned above, but also of quartz and small pyroxene crystals entrapped during crystal growth. Typically, low temperature alkali feldspars

were richer in potassium and we observed a tendency to evolve to albite-rich compositions with increasing temperature. Most plagioclase compositions were between albite and oligoclase. At 200MPa, the most Ca-rich plagioclase identified at 750°C with 2 wt.% initial H<sub>2</sub>O was An<sub>22</sub>. However, compositions with high An content (An<sub>60</sub>) were identified in runs at the same conditions if cordierite seeds were added to the homogenised hydrous glasses (Table 3). Those Ca-rich compositions were identified as rims around cordierite this indicating that cordierite may occur as a relict phase (Fig. 3F). The Ca-rich plagioclase is interpreted to be the result of a reaction of cordierite with

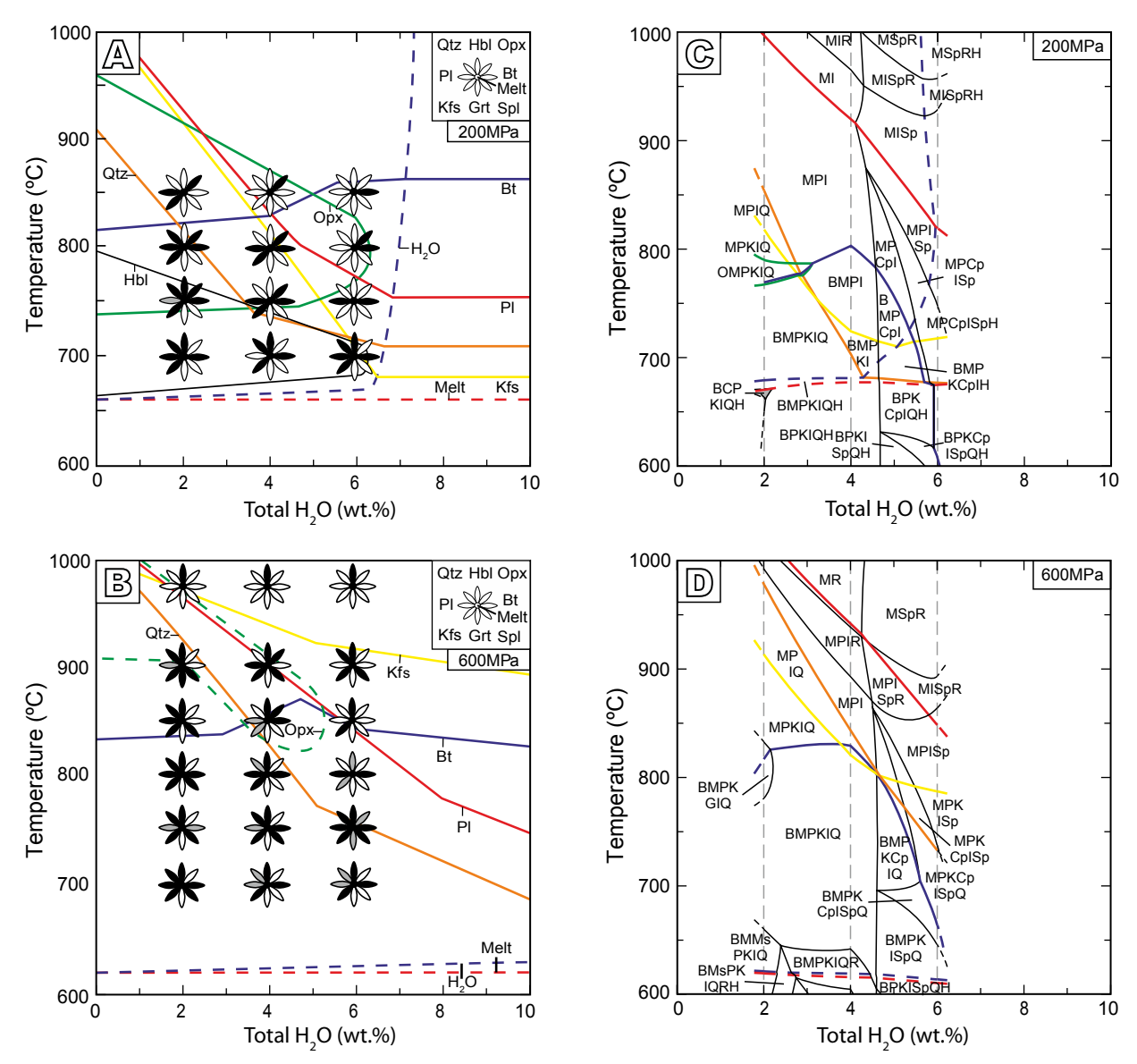


**FIGURE 5.** Experimentally determined phase relations (A and B) and corresponding calculated pseudosections (C and D). In A and B: for each experiment, at a given added water content and temperature, the corresponding symbol denotes if a phase was unambiguously identified (black field for the corresponding phase), if a phase was not observed (open field for the corresponding phase), if a phase is suspected but not clearly identified (gray field for the corresponding phase). Dashed lines are interpreted from comparable experiments in the literature. For the pseudosections in this figure and the following this is the abbreviation key: O: orthopyroxene; M: melt; Q: quartz, B: biotite, P: plagioclase; K: K- feldspar; G: garnet; I: ilmenite; R: rutile; C: cordierite; H: H<sub>2</sub>O; Ms: muscovite; S: sillimanite; Cp: clinopyroxene.

the melt. This observation demonstrates that cordierite is not a stable phase with the melt composition under those conditions, which will be discussed in detail below.

Accessory minerals were small and difficult to detect. Scarce ilmenite and titanite crystals were detected.

The compositions of the glasses varied mainly with temperature. Typical compositions are given for 200MPa in Table 4. The general behaviour is as follows: MgO concentrations were low (beyond the analytical resolution) and the FeO and TiO<sub>2</sub> decreased with decreasing temperature, as expected. SiO<sub>2</sub> generally increases with decreasing temperature, the opposite is observed for Al<sub>2</sub>O<sub>3</sub>. It is worth noting that the highest Al<sub>2</sub>O<sub>3</sub> concentration in glasses from experiments in which feldspars were observed was lower than 13.5 wt.% Al<sub>2</sub>O<sub>3</sub> and was systematically lower than that of the starting material (14.4) to 14.9 wt.%; Table 2). In contrast to  $K_2O$ , the  $Na_2O$  and CaO concentrations were systematically lower in glasses containing feldspars and their proportions determined the melt compositions. CaO decreased with the increase in the proportion of feldspars (i.e. decreasing temperature or decreasing water content).

#### Phase diagrams

The experimental results are shown in Figure 5 together with pseudosection phase diagrams for the VSCA starting materials at 200 and 600MPa. These pseudosections are described in the thermodynamic calculations section. In this kind of isobaric diagrams, in which phase stability fields are plotted as a function of the "added amount of water" and temperature, the shape of the stability curves for the different phases in the supersolidus region for the water-saturated field must be horizontal (Johannes and Holtz, 1996) and the volumetric proportion of the melt

phase does not change with increasing water content for a given temperature in this field. Our experiments were performed with added water between 2 and 6 wt.%. Depending on temperature and melt composition, watersaturated conditions at 200MPa are reached for ~5.6 to 6.1 wt.% H<sub>2</sub>O in the melt in rhyolitic to dacitic systems (e.g. Holtz et al., 1995; Moore, 1998). In addition, according to other published isobaric diagrams (Naney and Swanson, 1980; Clemens and Wall, 1981; Stern and Wyllie, 1981; Naney, 1983; Huang and Wyllie, 1986 and Carroll and Wyllie, 1990) for granitic systems, water saturation should be reached for higher initial added water contents than 6 wt.% at pressures above 200MPa. Thus, for the different pressures, an increase in volumetric melt proportion was monitored with increasing added water content from 2 to 4 to 6 wt.%. Nearly all our runs were water-undersaturated and fluid-absent, as determined after the experiments from weight loss after perforation of the capsule. The water saturation curve drawn in Figure 5A (200MPa) is only indicative and based on our knowledge of water solubility data. The water saturation curve is not indicated in Figure 5B (600MPa) because it is expected to be at a value higher than 10 wt.% H<sub>2</sub>O and a positive dependence of water solubility as a function of temperature is expected at this pressure (Holtz et al., 1995). Because the runs were performed at 700°C and above, all of them were situated in the supersolidus region. The solidus curves in the diagrams in Figures 5A and 5B were located taking into account data from watersaturated granitic peraluminous systems (Johannes and Holtz, 1996) which are relevant for the residual melts of the investigated composition.

The liquidus curves are not clearly constrained from the experimental dataset but the liquidus temperature increases with pressure at a given added water content, probably because of the increasing stability field of Cpx with pressure.

**TABLE 4.** Mean chemical composition of the glass phase at 200MPa, for different temperatures (°C) and initial water content (wt.%). Numbers in brackets represent number of analysis and calculated standard deviation values

T/H₂O <sub>i</sub>	700/2	700/4	700/6	750/2	750/4	750/6	800/2	800/4	800/6	850/2	850/4	850/6
	(11)	(14)	(11)	(5)	(5)	(6)	(15)	(15)	(23)	(20)	(19)	(19)
SiO <sub>2</sub>	69.45	70.62	70.57	73.79	72.11	70.79	73.00	70.70	69.21	71.71	69.46	66.73
	(0.71)	(0.34)	(0.45)	(1.03)	(0.37)	(0.68)	(0.58)	(0.26)	(0.74)	(0.39)	(0.33)	(0.95)
TiO <sub>2</sub>	0.17 (0.11)	0.10 (0.05)	0.15 (0.07)	0.13 (0.10)	0.14 (0.05)	0.22 (0.05)	0.24 (0.06)	0.22 (0.05)	0.28 (0.11)	0.36 (0.06)	0.38 (0.04)	0.37 (0.06)
Al <sub>2</sub> O <sub>3</sub>	11.73	11.64	11.73	12.01	12.27	12.75	12.46	13.32	13.69	13.27	13.93	14.16
	(0.32)	(0.38)	(0.26)	(0.63)	(0.25)	(0.18)	(0.22)	(0.20)	(0.29)	(0.19)	(0.22)	(0.46)
FeO	1.29 (0.33)	0.71 (0.17)	0.91 (0.15)	1.00 (0.31)	1.06 (0.23)	1.57 (0.32)	0.93 (0.23)	1.31 (0.04)	1.51 (0.40)	1.22 (0.19)	1.61 (0.23)	1.99 (0.25)
MgO	0.26 (0.16)	0.08	0.14 (0.12)	0.08 (0.03)	0.14 (0.06)	0.31 (0.16)	0.08 (0.03)	0.16 (0.04)	0.21 (0.12)	0.22 (0.03)	0.30 (0.05)	0.39 (0.07)
CaO	0.66	0.53	0.58	0.51	0.66	0.75	0.46	0.74	1.05	0.67	1.04	1.11
	(0.31)	(0.12)	(0.13)	(0.07)	(0.11)	(0.06)	(0.07)	(0.05)	(0.09)	(0.06)	(0.08)	(0.11)
Na₂O	3.02	2.84	3.00	2.82	3.26	3.31	3.08	3.65	3.77	3.56	3.70	3.76
	(0.28)	(0.20)	(0.21)	(0.45)	(0.32)	(0.14)	(0.36)	(0.47)	(0.25)	(0.29)	(0.27)	(0.29)
K₂O	4.29	4.38	4.44	4.94	4.62	4.41	5.05	4.38	4.03	4.78	4.34	4.17
	(0.28)	(0.13)	(0.15)	(0.32)	(0.19)	(0.19)	(0.11)	(0.15)	(0.19)	(0.22)	(0.16)	(0.16)
Total	90.90	90.94	91.56	95.30	94.26	94.12	95.32	94.51	93.79	95.84	94.78	92.70
	(0.75)	(0.60)	(0.39)	(1.22)	(0.32)	(0.97)	(0.63)	(0.51)	(0.54)	(0.51)	(0.67)	(0.61)

Cpx is the liquidus phase at 600MPa whereas Bt, Opx or Pl (depending on the added water content) are liquidus phases at 200MPa (Opx and Bt are the liquidus phases for 4 and 6 wt.% added water, respectively). The stability fields

of mineral phases in the water-undersaturated field were drawn by non-isothermic T-H<sub>2</sub>O limits (similar to diagrams in *e.g.* Naney (1983)). These stability fields of the main minerals are detailed below.

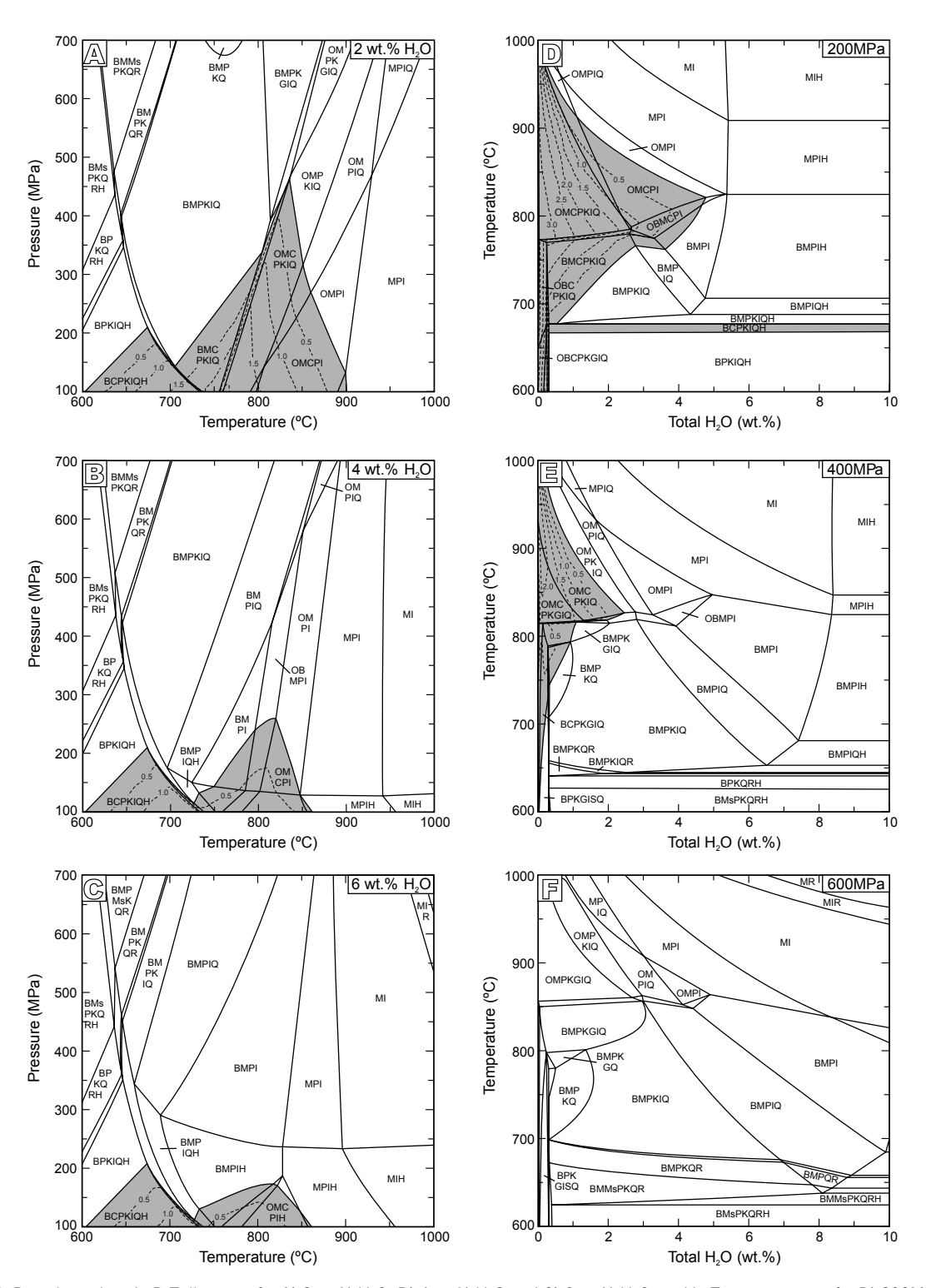


**FIGURE 6.** Pseudosections in P-T diagrams for A) 2 wt.%  $H_2O$ , B) 4 wt.%  $H_2O$  and C) 6 wt.%  $H_2O$ , and in T-water content for D) 200MPa, E) 400MPa and F) 600MPa. Stability fields of subsolidus cordierite and cordierite in equilibrium with melt are showing in gray with contour lines, which predict a very low amount of cordierite in equilibrium with the melt.

Clinopyroxene is present in all the experiments performed at 400 and 600MPa and its saturation curve is above the investigated temperature. Its stability field is difficult to determine unambiguously, because this phase was already present in the starting materials (synthesis from the 975°C experiments). The clinopyroxene dissolution texture observed in the low temperature experiments may indicate that this phase is a relict and may not be stable, as expected from the comparison with other phase diagrams (Naney, 1983; Clemens *et al.*, 1986).

Orthopyroxene was a stable phase at the three studied pressures. At 200MPa this phase showed a larger stability field than at higher pressures. The stability curves drawn in Figure 5 indicate that orthopyroxene was probably not stable at low temperature and at water activities close to 1 in the water saturated region of the diagrams for any studied pressure.

The biotite saturation curve has a similar shape in both diagrams, with a possible maximum at intermediate water contents. Garnet and spinel were interpreted as metastable in our experiments (the minerals were always rimed by other phases) and, consequently, their stability fields are not included in the phase diagrams of Figure 5. Similar ferromagnesian phases (Opx±Cpx and Bt) have been described in previous studies using metaluminous or granodioritic compositions, including A-type granitic and rhyolitic compositions (e.g. Naney 1983; Dall'agnol,

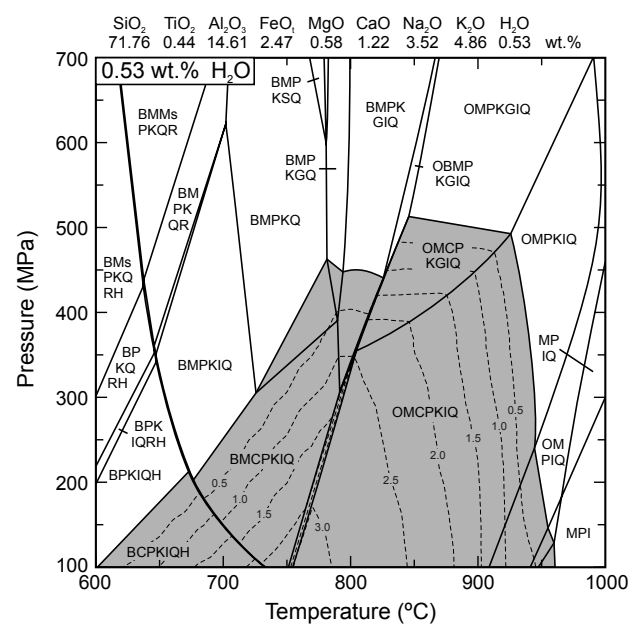


**FIGURE 7.** P-T pseudosection for the analysed water content of the selected cordierite monzogranite of Cabeza de Araya (sample GC28069603) (see Table 2). Stability fields of subsolidus cordierite and cordierite in equilibrium with melt are showing in gray with contour lines.

1999; Klimm *et al.*, 2003; Almeev *et al.*, 2012; Scaillet *et al.*, 2016). The absence of muscovite and stable garnet is explained by the bulk composition used in this study, which is less Al-rich and slightly more Fe- and Mg-rich than the granite compositions investigated by Huang and Wyllie (1973), Stern and Wyllie (1981), Huang and Wyllie (1986) and Scaillet *et al.* (1995), although the metastable presence of mentioned Al-rich minerals may have also affected the crystallization of muscovite.

Alkali feldspar was clearly more often identified than plagioclase, but this last mineral was most probably not identified in several runs because of the high crystallinity (the runs at 400 and 600MPa with the lowest added water contents) because the already explained difficulty to distinguish these phases in BSE images. The same observation can be done for quartz. In these runs with low melt fraction, there was a strong nucleation and tectosilicates tend to crystallize as tiny intergrowths. Experiments in which tectosilicate phases are expected but which could not be unambiguously detected are indicated in Figure 5 (the presence of such phases is marked by a gray symbol in Fig. 5). For example, quartz was not identified at low temperature at 400 and 600MPa, which is unrealistic, considering that it was present in runs at higher temperature (same added water content). The temperature of crystallization of alkali feldspar decreases with increasing added water content, as expected from previous studies. For a given added water content, tectosilicates, and especially alkali feldspar, start to crystallize at higher temperature at 600MPa than at 200MPa. Apart from a possible effect of pressure, this behaviour can be expected considering that the water activity should be higher at 200MPa than at 600MPa, for a given amount of added water (as a result of the effect of pressure on water solubility).

#### THERMODYNAMIC CALCULATIONS

To establish the stability field of magmatic cordierite in the cordierite monzogranite chosen for this study in Cabeza de Araya (Table 2), T-H<sub>2</sub>O and P-T pseudosections were constructed using the software PERPLE\_X, version 6.7.1, the hp02ver.dat database (Holland and Powell, 1998, and successive updates) and the solution\_model. dat database for the activity models of the mineral and melt solutions (Connolly, 2005, 2009). A list of the solution models chosen for the pseudosections is given in Electronic Appendix I (available at www.geologica-acta. com). Two sets of compositions were used for the T-H<sub>2</sub>O pseudosections: one was the composition of the glasses used in the experimental runs for each different water content (Fig. 5C; D), and the second set was the anhydrous composition for the cordieritic monzogranite GC28269603

(Table 2) with variable amounts of water (Fig. 6D; E; F). For simplicity, all Fe was considered to be only FeO (*i.e.* the calculations were made in the NCKFMASHT system), which records oxygen fugacity conditions of -14 at 850°C or QFM+0, similar to those of experimental runs made in the piston-cylinder apparatus (Patiño Douce and Beard, 1995).

Pseudosections shown in Figure 6 indicate that magmatic cordierite is always a minor phase. In the T-H<sub>2</sub>O pseudosections using the GC28269603 composition at 400 and 200MPa, the maximum amount of magmatic cordierite is 2.3 vol.% and 3.4 vol.%, respectively, always at very low H<sub>2</sub>O contents (Fig. 6C; D), and by 6 wt.% total H<sub>2</sub>O it is almost completely absent (Fig. 6F). In the T-H<sub>2</sub>O pseudosections using the experimental glass compositions, no cordierite is predicted, in agreement with the experimental results (Fig. 5A; B). Also, the stability of cordierite decreased with increasing pressure, with the highest concentrations at 100MPa for each bulk H<sub>2</sub>O content, and being completely absent P>500MPa (Fig. 6A; C; E). The predicted amount of magmatic cordierite at 200MPa, the lowest experimental pressure, is 2.9 vol.%, again very low.

Given the close relationship between total  $H_2O$  content and the amount of magmatic cordierite, and considering that the amount of this phase is higher for very low  $H_2O$  contents, a new pseudosection was calculated using the analyzed  $H_2O$  amount of the Cabeza de Araya sample chosen for the experimental study, 0.53 wt.%  $H_2O$ . Under these new conditions, the highest amount of cordierite

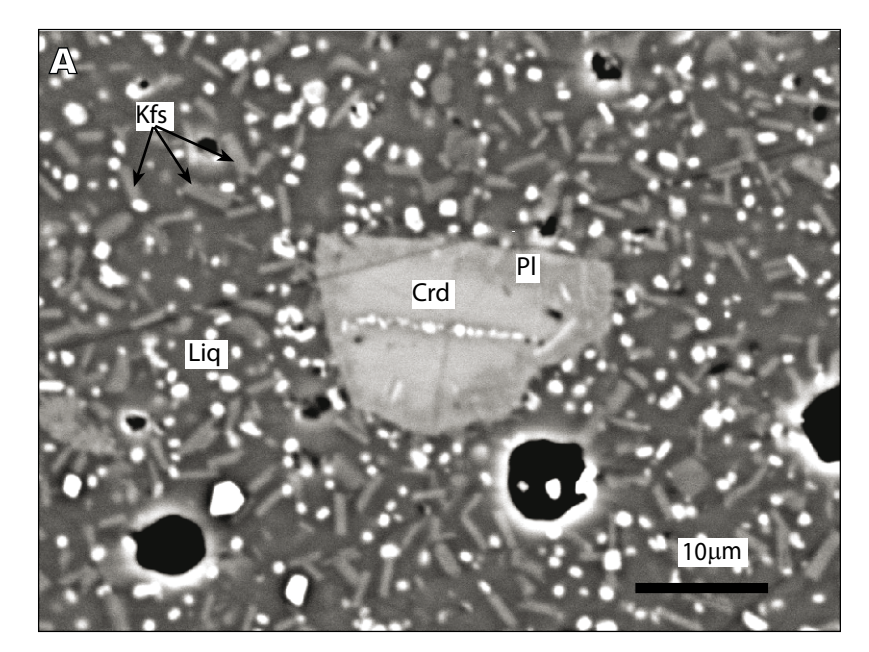
is again at 100MPa (3.1 vol.%) and this amount is again virtually zero for P>500MPa (Fig. 7).

In summary, magmatic cordierite is predicted to be stable for certain experimentally tested P-T conditions albeit always in very low amount, always below 3.5 vol.%. This extremely low amount of cordierite may have been present in the low temperature and low H<sub>2</sub>O content (and thus mineral-rich) experiments. If this phase was not found in the experimental runs, this may have been caused by the inherent difficulties of identifying very low amount of mineral phases at the experimental P-T conditions, despite the fact that the runs, have been thoroughly studied under the SEM.

#### DISCUSSION

#### Attainment of equilibrium and stability of cordierite

We consider that the experimental approach used in this study is the most appropriate to check for the stability of cordierite. Melting experiments using powdered granite are not appropriate for the determination of phase equilibria (the core of relict phases may not react with the surrounding silicate melt; see also Pichavant *et al.*, 2007). The use of pre-equilibrated material (600 and 400 MPa) or of glass powder (200MPa) is appropriate to test if a mineral phase is in equilibrium with a melt having a composition close to that of the bulk rock, provided that there are no nucleation problems for this phase.



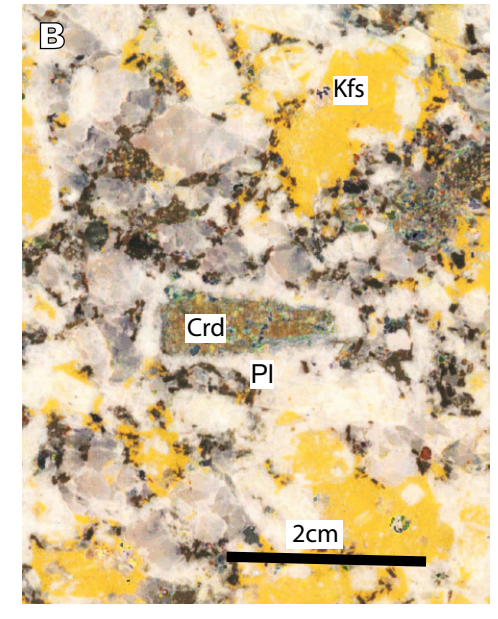


FIGURE 8. A) Experimental product showing cordierite rimmed by plagioclase and B) natural occurrence of the same rim in a Cabeza de Araya slab.

Cordierite is a mineral phase stable under very different conditions varying from metamorphic environments, including crustal anatexis (Patiño-Douce and Beard, 1995; Kalt et al., 1998; Harley et al., 2001), to magmatic, pegmatitic and metasomatic fields (Clarke, 1995). Cordierite was observed in a number of experiments in which this mineral phase nucleated from a silicate melt (e.g. Holtz and Johannes, 1991; René, et al., 2008) and the nucleation of cordierite is not particularly problematic. Pilot experiments with the chosen starting materials were also performed at different durations (after 24 hours at 950°C, the duration of the second step at lower temperature varied from 24 to 96h) to check for equilibrium conditions and the detected phase assemblages were identical, independently on the time. In this study, several types of experiments have been useful to prove the cordierite disequilibrium with the chosen bulk composition.

Considering that thermodynamic calculations predict that very small amounts of cordierite (or garnet) may be present at equilibrium conditions, the experiments at 400 and 600MPa and some experiments at 200MPa were doped with small seeds of natural cordierite and garnet. Thus, even if nucleation problems may occur, the analysis of the experimental products (evidence for growth or dissolution of seeds) should clearly indicate if the added mineral phases are in equilibrium or not with the surrounding melt. At 400 and 600MPa, cordierite was never observed in the run products (note that this may be due to the first heating stage at 975°C, which may lead to a complete dissolution of the seeds) and selected experiments performed with and without added seeds yielded similar products (García-Moreno, 2004). The experiment containing cordierite seeds at 200MPa was conducted at 750°C and 4 wt.% added H<sub>2</sub>O (conditions at which cordierite could be stable from the thermodynamic calculation). In this case a reaction rim composed of Ca-rich plagioclase could be observed (growth of Pl over relict cordierite cores; Figs. 3F and 8A), clearly indicating that cordierite is not stable at such conditions. A reaction such as Crd+Ca-melt → Ca-Pl can be formulated to explain this textural observation. In order to check for the possibility of plagioclase nucleation problems in this experiment, another experiment was performed with seeds of plagioclase and cordierite under the same conditions. Plagioclase seeds were neither dissolved nor recrystallized from the melt phase, but the cordierite seeds still reacted with the melt to produce rims composed of plagioclase.

Experiments with a mixture of  $\rm H_2O$  and  $\rm CO_2$  as fluid phase under the same P-T conditions with and without added cordierite seeds were also performed. The mineral assemblage was similar to that of the experimental products obtained in samples with pure  $\rm H_2O$  as added fluid phase, so the absence or presence of  $\rm CO_2$  in the system did not control the crystallization of cordierite.

Thus, although nucleation problems cannot be completely excluded, several observations indicate that cordierite is not expected to be a stable phase over a wide P-T-added  $\rm H_2O$  range in the investigated conditions. Thermodynamic calculations agree with this conclusion, as they predict only a very small amount of cordierite. These thermodynamic calculations also show that even though different  $\rm fO_2$  conditions may change the ferromagnesian phase relations, for our composition and experimental conditions, these relations are not significantly modified. It would be interesting to check the influence of different  $\rm fO_2$  conditions also in the experiments.

In addition, the presence of some elements that were not considered in the experimental and the numerical approach, like boron, chlorine and ammonium, may play a role in the stability of cordierite. Such elements could be provided by the metapelitic protolith in the generation of granitic melt, thus modifying the P and T conditions to values below what would be normal for the generation of these granitic bodies and so affecting the phase relations. Hall et al. (1996) described a clear correlation between the amount of NH<sub>4</sub> in the rock and its peraluminosity, shedding light on partial melting and magmatism related to the presence of volatiles and cordierite. However, although experiments with these additional components would be interesting for a future work, there is no available information indicating that such elements would influence strongly the stability field of cordierite at the scale of a pluton such as the Cabeza de Araya.

## Cordierite meaning and origin of Cabeza de Araya cordierite monzogranites - granodiorites

The absence of cordierite as a stable phase in our experiments and thermodynamic calculations is a key point to the understanding of the origin of the monzogranites investigated in this study. According to numerous data obtained from melting experiments of plausible protoliths for the Iberian peraluminous granites (*e.g.* Green, 1976; Holtz and Johannes, 1991; Vielzeuf and Montel, 1994; Castro *et al.*, 1999; Corretgé *et al.*, 2001) in which cordierite was present as a stable phase, it could be expected that this mineral is also among the stable phases in the investigated composition of this study, even if it has been demonstrated that this type of granites are not pure products of partial melting of Al-rich protoliths.

The experimental results at 200MPa and 750°C with added cordierite seeds leading to the formation of plagioclase rims with high An content (An<sub>60</sub>), contrasting with the low An content (maximum value is An<sub>22</sub>) of the other synthesized plagioclases, clearly indicate that cordierite is a reactant phase and that the local high Al concentration (resulting from the breakdown of cordierite)

results in the formation of a Al- and Ca-rich plagioclase. Interestingly, the breakdown reaction of cordierite yielding to the formation of plagioclase in the presence of melt, although not often described in natural case studies, can be observed in the cordierite monzogranites of Cabeza de Araya (Fig. 8B). Scarce evidences of this kind of cordierite reaction has also been described in the Deddick granodiorite by Maas (1997) and in the Cerro del Hoyazo dacite by Zeck (1992). In the latter case, cordierite may be introduced in a Ca-rich dacitic magma by mingling processes and may remain as a metastable phase in the system as a result of a short residence time in the magma prior to eruption. These observations confirm that cordierite may not be able to crystallize or grow from a relatively Ca-rich metaluminous melt over most of the crystallization interval. Therefore, the composition of the rock under study may not represent a primary liquid, or a pure liquid produced from the partial melting of a rock. The presence of cordierite crystals in strong disequilibrium with its magmatic host was also deduced from the study of a monzogranitic body from the Spanish Central System (Gredos massif) with similar geochemical composition than the Cabeza de Araya monzogranite (Díaz-Alvarado et al., 2011). In the light of the experimental results, other processes or conditions need to be considered for the formation of magmatic cordierite as observed in the natural Cabeza de Araya cordierite monzogranites.

An alternative for other conditions that we have not tested is that cordierite may crystallize at very low pressure and low fO<sub>2</sub>. Our experiments performed at 200MPa were done under relatively oxidizing conditions (NNO-NNO+1). Cordierite may crystallize at 200MPa but at lower fO<sub>2</sub> as indicated by results of Scaillet et al., (1995) in which cordierite crystallized at low fO2 and low water content (but at 400MPa) in a tourmaline-muscovite leucogranite (GB4) with a bulk Al<sub>2</sub>O<sub>3</sub> content that is just 0.3 wt.% higher than VSCA6. However, as we described before, the thermodynamic calculations made with different  $fO_2$ do not indicate that  $fO_2$  may control strongly the stability of cordierite. In addition, as mentioned above, volatile composition different to H2O and CO2, may influence the phase relations and it could be interesting to check in future experiments how they can influence cordierite stability in this kind of magmas.

# Cordierite as an equilibrium magmatic phase at pressure <200MPa and temperature close to the solidus

The pseudosections cannot reproduce fruitfully the experimental results (White *et al.*, 2011). However, because the selected thermodynamic database is well suited for peraluminous systems only a small deviation between the calculated phase assemblages and the experimentally

determined phase assemblages may be expected. The amount of cordierite predicted by the pseudosections is low (<3.5 vol.%) and a small variation of the bulk chemical composition may be sufficient to reconcile experimental and calculated data. Thus, the calculated phase assemblages can be used qualitatively to explore the conditions at which cordierite may become an equilibrium phase in the investigated composition.

The pseudosections in Figure 6 show that cordierite is barely a stable phase at temperature just above the solidus at low pressure, when the conditions are close to be water-saturated and at high crystallinity. This implies that cordierite is not predicted to be a late magmatic phase. This is in agreement with the petrographic observations of prismatic cordierite in the Cabeza de Araya monzogranites, which has been interpreted as an early crystallizing phase in numerous cordierite granites (Barbey *et al.*, 1999; Rapela, 2002; Sandeman and Clark, 2003 and references therein). We have better interpreted cordierite crystallization as an exo-peritectic phase in many cases.

The pseudosections in Figure 6 also indicate that cordierite could become a stable phase at high temperature (low crystallinity of the magma), well above the solidus, if pressure is lower than 200MPa. Following Figure 6, cordierite should be a stable phase over a temperature interval of ~100-150°C at pressures of 150 to 100MPa (assuming low water activities). This would imply that magma chambers in which cordierite-bearing monzogranites crystallized were very shallow. The presence of andalusite as accessory phase in some samples confirms the low pressure of crystallization. To our knowledge, no experiments have been performed to test the hypothesis of a very shallow crystallization (150 to 100MPa).

#### Processes for the formation of cordierite granites (s.l.)

The conditions of formation of cordierite in the Hercynian granites *s.l.* of Spain has been discussed for a long time. Three main hypotheses have been proposed (*e.g.* Ugidos and Recio, 1993; Ugidos *et al.*, 2008; Díaz-Alvarado *et al.*, 2011): i) cordierite is already present in the contaminant as a metamorphic phase, ii) cordierite is a phase formed by incongruent melting of the contaminant prior to or during its incorporation into the magma or iii) cordierite forms in local domains of the magma containing high proportions of contaminant as a result of a peritectic reaction which controls the nucleation of cordierite.

Considering the heterogeneity of possible contaminants (Ugidos *et al.*, 2008) as well as different possible degrees of partial melting in the contaminants (depending on temperature, water activity), the three mechanisms are possible and do probably occur in the natural systems.

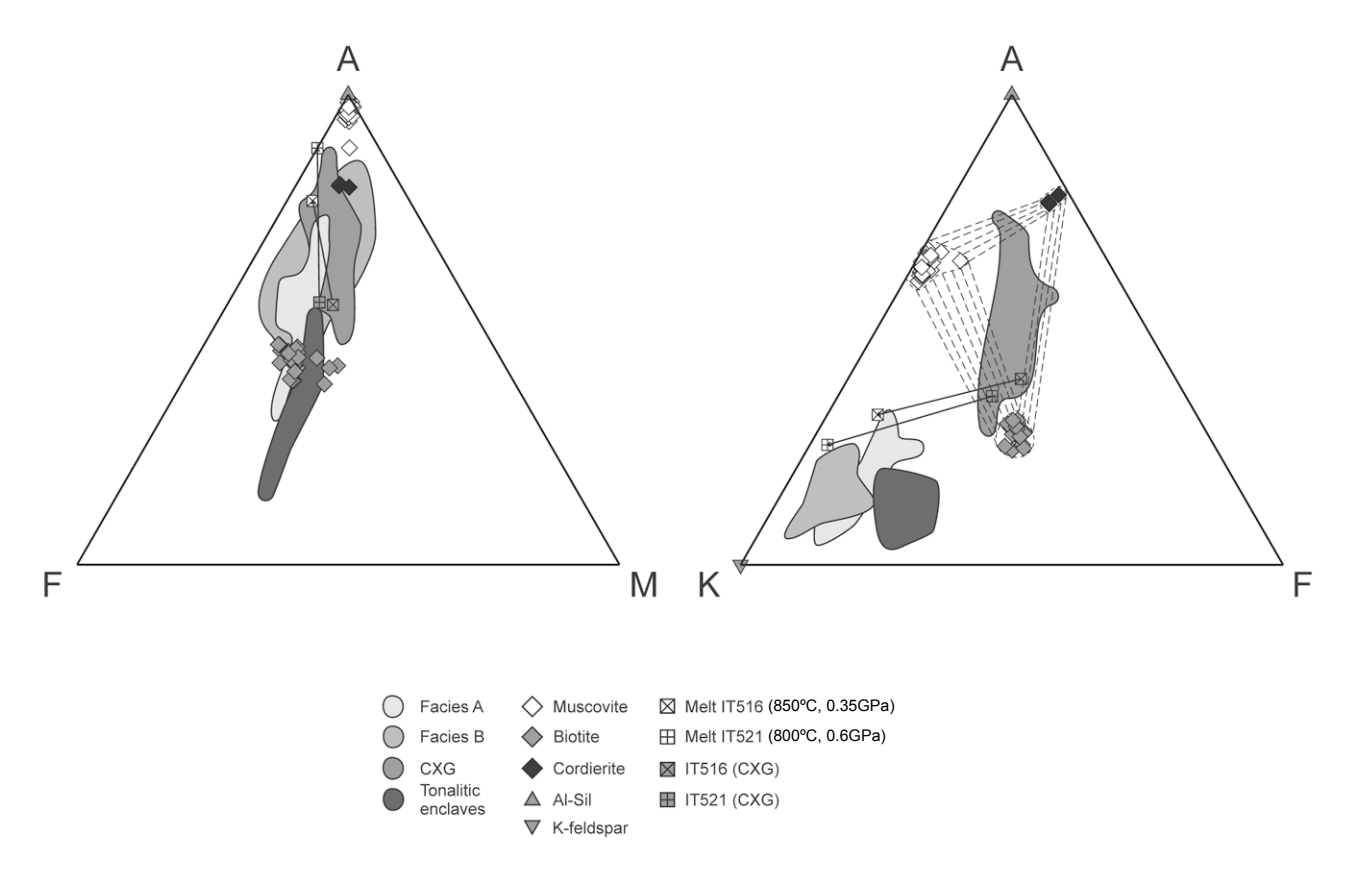


FIGURE 9. AFM and AKF diagrams showing the relations of the different Cabeza de Araya facies with melts generated in partial melting experiments of CXG rocks.

The second scenario is documented by the formation of cordierite in partial melting experiments of peraluminous pelites or gneisses at different pressure conditions (Hoffer and Grant, 1980; Holtz and Johannes, 1991; Carrington and Harley, 1995; Erdmann *et al.*, 2007). Partial melting experiments performed with a hornfels from the Schistgreywacke Complex (CXG), which can be considered a possible protolith of the Cabeza de Araya rocks (Corretgé *et al.*, 2001), produced newly formed cordierite in equilibrium with a relatively Ca-rich melt (with *ca.* 1.3% CaO) compared to other partial melt produced under similar conditions and with similar starting materials (Castro *et al.*, 1999).

The third scenario may be evoked from the experimental observations of Díaz-Alvarado *et al.* (2011), who proposed that cordierite forms in local domains as a result of a peritectic reaction that controls the nucleation of cordierite. A possible peritectic reaction Bt + Qtz + Pl + Als  $\rightarrow$  Crd + Kfs + melt was proposed by these authors, the Als phase being provided by the contaminant. In any case, Al<sub>2</sub>O<sub>3</sub> and most probably CaO activity play a fundamental role on the presence or absence of cordierite at magmatic conditions. In light of the experimental results and the textural evidences, we can conclude that some cordierite precipitation comes from the assimilation of pelitic material, as it has already

been described in previous studies (Díaz-Alvarado *et al.*, 2011; García-Moreno *et al.*, 2007). In the case of Cabeza de Araya batholith, an exogenous character can be identified because cordierite stabilization is the result of an exo-peritectic reaction related to the incongruent melting of pelitic xenoliths. These xenoliths were dragged from the walls during the magma ascent and remained as relicts of the assimilation process, located in the marginal facies of the Cabeza de Araya batholith (Facies A). The further peritectic reaction, promoted by an input of late-magmatic fluids, gave rise to cordierite prismatic crystals surrounded by biotite (Fig. 2).

Cordierite is expected to be stable in the Cabeza de Araya magmas only if the  $Al_2O_3$  in the melt is high enough. Considering that cordierite did not crystallize from the bulk composition GC28069603, this indicates the  $Al_2O_3$  concentration and probably the  $Al_2O_3$ /CaO ratio in the melt after the assimilation process was higher than that in the experimental products. The main parameter controlling the crystallization of cordierite, as can be deduced from a comparison of previous data obtained in systems in which the melt coexists with plagioclase and cordierite is the  $Al_2O_3$  content of the melt (or its peraluminous character). Our data (Table 3) indicate that  $Al_2O_3$  contents in the melt of ~12.5 wt.% are too low for cordierite to crystallize in

the temperature range 700-800°C. In the same temperature range, crystallization and melting experiments indicate that cordierite and plagioclase coexist in a felsic melt with at least 13.5 wt.% Al<sub>2</sub>O<sub>3</sub> (e.g. Holtz and Johannes, 1991; Castro et al., 1999; René et al., 2008; Díaz-Alvarado et al., 2011). We conclude that the peraluminous character and the Al<sub>2</sub>O<sub>3</sub>/CaO of the reactive composition of the Cabeza de Araya magma was higher than that of the bulk composition, implying that part of the Ca-Al-bearing phases (plagioclase) were not equilibrated with the magma during and after assimilation. The possible origin of this "non-reactive plagioclase" is discussed below.

### Role of mingling/mixing processes with mafic magmas prior to assimilation

The projection of the Cabeza de Araya plutonic rocks and of possible Al-rich contaminant in the AKF and AFM diagrams (Fig. 9) confirms that the compositions of the Facies A (cordierite-bearing monzogranites-granodiorites) cannot derive only from the assimilation of hornfels or peraluminous metasediments from the Schist-greywacke Complex by Facies B-type rocks (cordierite-free). As in most of the granodiorites from the Iberian Peninsula, the presence of mafic to tonalitic enclaves are also observed in Cabeza de Araya cordierite-bearing monzogranitesgranodiorites and these rocks are often cogenetic with hornblende-bearing diorites and biotite-bearing Ca-rich rocks (tonalites), typical of calc-alkaline magmatism. This post-orogenic calc-alkaline magmatism would be related to basic melt generated by post-collisional adiabatic decompression of the mantle and uprising geotherm, together with crustal thining evolution (Carracedo et al., 2009). In such type of magmas hybridization processes and mingling processes between mafic enclaves and more felsic magmas have been documented (see García-Moreno et al., 2006 and 2007, for the Cabeza de Araya pluton). This hybridization process can modify locally the Al<sub>2</sub>O<sub>3</sub> and CaO activities in the magmas and can lead to the incorporation of mafic phases and plagioclase via mingling processes in the magma.

Considering that the experimental results clearly indicate that only part of the magmatic assemblage was involved as the reactant magma during the assimilation process of Al-rich material, a possible scenario explaining the presence of euhedral cordierite crystals in the monzogranites-granodiorites is that a significant fraction of plagioclase was already present during assimilation but was chemically isolated from the reactive assemblage. This amount of "non-reactive plagioclase" can be extremely high if mingling processes occurred with mafic melt just prior to assimilation of Al-rich rocks. Thus, the presence of cordierite in such Ca-rich granodioritic systems suggests that the host magmas have a high crystallinity and that only

a part of the crystals are in equilibrium with the silicate melt. Other phases than plagioclase may also act as "nonreactive phases". However, the equilibration of plagioclase requires interdiffusion processes (Al+Ca ↔ Na+Si) which are slow when compared to the diffusion processes in other minerals which may be present in the calc-alkaline magmas (biotite, alkali feldspar, hornblende). Finally, considering that the temperature of assimilated rocks surrounding magma chambers is expected to be lower or identical to the host magma, assimilation processes are not expected to lead to an increase of the melt fraction in the bulk system, implying that the fraction of "non-reactive" plagioclase is not expected to change strongly in the course of assimilation. Experimental and natural evidence in the case of Cabeza de Araya cordierite-monzogranites also shows that assimilation may lead to the crystallization of plagioclase when cordierite is not stable.

The observation of cordierite rimmed by An-rich plagioclase may also indicate that the mingling/mixing processes in the calc-alkaline magmas do not necessarily occur a long time prior to the assimilation of Al-rich rocks. Clearly, in some domains of the magma chamber, cordierite was initially stable before the beginning of its breakdown reaction. This would indicate that an equilibration of the calc-alkaline magma is occurring after the assimilation processes or that mixing with mafic end-members occurred simultaneously or after the assimilation of Al-rich rocks. An increase in water activity could also lead to a preferential dissolution of plagioclase crystals compared to biotite and quartz (García-Moreno et al., 2006), leading to a variation of the Al<sub>2</sub>O<sub>3</sub>/CaO of the reactive composition. The presence of Rapakivi texture may also indicate that several magma pulses occurred in the Cabeza de Araya chamber. Such replenishment processes may also lead to a local temperature increase favouring the assimilation of surrounding hornfelses and peraluminous metasediments and complex reactions between metaluminous and peraluminous magma batches. Finally, in contrast with other examples studied in the Iberian Massif (Ugidos et al., 2008), there is no field evidence for assimilation of surrounding rocks at the level of emplacement. Thus, the local increase in Al activity in the Cabeza de Araya magma chamber leading to the formation of cordierite must have occurred at deeper levels, which is a further indication for possible simultaneous assimilation and hybridization processes.

In summary, if mineral phases that are not in equilibrium with the bulk assemblage, such as cordierite in the present study, are not identified, the existence of such crystal mushes recording magma mixing processes is often difficult to identify unequivocally in plutonic systems because there is a long time span between mixing event and the solidus (leading to re-equilibrations of the magmatic

minerals). However, it has been more clearly documented in dacitic to rhyolitic volcanic systems (e.g. Nakamura, 1995, Nakada and Motomura, 1999; Bachmann et al., 2002, Parmigiani et al., 2014). In the case of the Cabeza de Araya, the temporal gap between the mixing/mingling of felsic and mafic calk-alkaline magmas and the assimilation of Al-rich rocks may be small and both processes may have occurred simultaneously. In this sense, a complex assimilation and hybridization process is necessary to explain the generation of the cordierite monzogranites.

#### **CONCLUSIONS**

Cordierite could not be reproduced in crystallization experiments and thermodynamic calculations at 600, 400 and 200MPa, using a synthetic analogue of cordieritebearing monzogranites of the Cabeza de Araya. This may indicate either that the experimental conditions were not realistic or that the phases in the investigated sample are not in chemical equilibrium. The first hypothesis could be tested by crystallization experiments conducted at pressures lower than 200MPa and also for different fO<sub>2</sub> at low temperature. However, it seems not realistic that a large magma chamber such as that of the Cabeza de Araya may have been located at depths corresponding to a lithostatic pressure 150MPa or less. The second hypothesis implies that cordierite crystallized from a melt that was not in equilibrium with part of the mineral assemblage present in the magma. The silicate melt from which cordierite crystallized was more Al-rich than the melt composition that would be in equilibrium with the bulk composition, which may result from assimilation and partial melting processes of metasediments from Schist-greywacke Complex. Textural evidences also confirm the assimilation hypothesis as the precursor of cordierite stabilization by an exo-peritectic reaction. The geochemical and petrographic observations indicate that the mineral assemblage that does not equilibrate with the Al-rich melt is mainly composed of plagioclase. The presence of significant amounts of "non-reactive" plagioclase may be explained by hybridization processes (mixing/mingling) typical in calk-alkaline magmas, resulting in the formation of a crystal mush which never reaches bulk equilibrium.

#### **ACKNOWLEDGMENTS**

This work forms part of the PhD. thesis of Olga García-Moreno, with help of the Principado de Asturias by a predoctoral grant. Financial support for the experiments comes from the Spanish MEC and MCYT projects: PB97-0439, BTE2001-2769, LGC2004-06808-C04 as well as from the German Science Foundation (project HO1337/22). Carmen Rodriguez is grateful

to her post-doctoral grant from the University of Huelva. We would like to thank Antonio Castro for the discussion about the phase relations and cordierite meaning in Cabeza de Araya rocks.

#### **REFERENCES**

- Almeev, R., Bolte, T., Nash, B., Holtz, F., Erdmann, M., Cathey, H., 2012. High temperature, low H<sub>2</sub>O silicic magmas of the Yellowstone hotspot: an experimental study of rhyolite from the Bruneau-Jarbidge eruptive center. Journal of Petrology, 53, 1837-1866.
- Amice, M., 1990. Le complexe granitique de Cabeza de Araya (Estrémadure, Espagne): zonation, structures magmatiques et magnétiques, géométrie, discussion du mode de mise en place. PhD Thesis, Toulouse, Université de Toulouse III, 225pp.
- Amice, M., Bouchez, J.L., Aranguren, A., Alvarez, F., Vigneresse, J.L., 1991. El batolito granítico de Cabeza de Araya (Extremadura): comparación de sus estructuras magmáticas y magnéticas. Boletín Geológico y Minero, 102(3), 455-471.
- Audrain, J., Amice, M., Vigneresse, J.L., Bouchez, J.L., 1989. Gravimetrie et geometrie tri-dimensionelle du pluton granitique de Cabeza de Araya (Estremadure, Espagne). Comptes Rendus de l'Académie des Sciences de Paris, Série II, 309, 1757–1764.
- Bachmann, O., Dungan, M.A., Lipman, P.W., 2002. The Fish Canyon magma body, San Juan volcanic field, Colorado: rejuvenation and eruption of an upper-crustal batholith. Journal of Petrology, 43(8), 1469-1503.
- Barbey, P., Marignac, C., Montel, J.M., Macaudière, J., Gasquet, D., Jabbori, J., 1999. Cordierite growth texture and conditions of genesis and emplacement of crustal granitic magmas: the Velay Grante Complex (Massif Central, France). Journal of Petrology, 40, 1425-1441.
- Bea, F., 2004. La naturaleza del magmatismo de la Zona Centro Ibérica: consideraciones generales y ensayo de correlación. In: Vera, J.A. (ed.). Geología de España, Sociedad Geográfica Española - Instituto Geológico y Minero de España (SGE-IGME), Madrid, 128-133.
- Botcharnikov, R.E., Koepke, J., Holtz, F., McCammon, C., Wilke, M., 2005. The effect of water activity on the oxidation and structural state of Fe in a ferro-basaltic melt. Geochimica et Cosmochimica Acta, 69(21), 5071-5085.
- Capdevila, R., 1969. Le métamorphisme régional progressif et les granites dans le segment hercynien de Galice Nord Orientale (NW de l'Espagne). PhD Thesis, Montpellier, Université de Montpellier, 430 pp.
- Capdevila, R., Corretgé, L.G., Floor, P., 1973. Les granitoïdes varisques de la Meseta ibérique. Bulletin de la Societé Geológique de France, (7) XV (3-4), 209-228.
- Carracedo, M., Gil Ibarguchi, J.I., García de Madinabeitia, S., Berrocal, T., 2005. Geocronología de los granitoides hercínicos de la Serie Mixta: Edad U-Th-Pbtotal de monacitas del Plutón de Cabeza de Araya (Zona Centroibérica) y de las manifestaciones filonianas asociadas. Revista de la Sociedad Geológica de España, 18(1-2), 77-88.

- Carracedo, M., Paquette, J.L., Alonso Olazabal, A., Santos Zalduegui. J.F., de García de Madinabeitia, S., Tiepolo, M., Gil Ibarguchi, J.I., 2009. U-Pb dating of granodiorite and granite units of the Los Pedroches batholith. Implications for geodynamic models of the southern Central Iberian Zone (Iberian Massif). International Journal of Earth Sciences (Geologische Rundschau), 98(7), 1609-1624.
- Carrington, D.P., Harley, S.L., 1995. Partial melting and phase relations in high-grade metapelites: an experimental petrogenetic grid in the KFMASH system. Contributions to Mineralogy and Petrology, 120, 270-291.
- Carroll, M.R., Wyllie, P.J., 1990. The system tonalite-H<sub>2</sub>O at 15kbar and the genesis of calc-alkaline magmas. American Mineralogist, 75, 345-357.
- Castro, A., 1984. Los granitoides y la estructura hercínica de Extremadura Central. PhD Thesis, Salamanca, Universidad de Salamanca, 202pp.
- Castro, A., 1985. The Central Extremadura Batholith: Geotectonic implications (European Hercynian belt)-An outline. Tectonophysics, 120, 57-68.
- Castro, A., Patiño, E., Corretgé, L.G., de la Rosa, J., El-Biad, M., El-Hmidi, H., 1999. Origin of peraluminous granites and granodiorites, Iberian massif, Spain: an experimental test of granite petrogenesis. Contributions to Mineralogy and Petrology, 135, 255-276.
- Clarke, D.B., 1995. Cordierite in felsic igneous rocks: a synthesis. Mineralogical Magazine, 59, 311-325.
- Clemens, J.D., Wall, V.J., 1981. Origin and crystallization of some peraluminous (S-type) granitic magmas. Canadian Mineralogist, 19, 111-131.
- Clemens, J.D., Holloway, J.R., White, A.J.R., 1986. Origin of an A-type granite: experimental constraints. American Mineralogist, 71, 317-324.
- Connolly, J.A.D., 1990. Multivariable phase diagrams: an algorithm based on generalized thermodynamics. American Journal of Science, 290(6), 666-718.
- Connolly, J.A.D., 2005. Computation of phase equilibria by linear programming: A tool for geodynamic modeling and its application to subduction zone decarbonation. Earth and Planetary Science Letters, 236(1-2), 524-541.
- Connolly, J.A.D., 2009. The geodynamic equation of state: What and how. Geochemistry, Geophysics, Geosystems, 10(10), Q10014, 19pp.
- Connolly, J.A.D., Petrini, K., 2002. An automated strategy for calculation of phase diagram sections and retrieval of rock properties as a function of physical conditions. Journal of Metamorphic Geology, 20(7), 697-708.
- Corretgé, L.G., 1971. Estudio petrológico del Batolito de Cabeza de Araya (Cáceres). PhD Thesis, Salamanca, Universidad de Salamanca, 453pp.
- Corretgé, L.G., Suárez, O., 1994. A garnet-cordierite granite porphyry containing rapakivi feldspars in the Cabeza de Araya batholith (Extremadura, Spanish Hercynian belt). Mineralogy and Petrology, 50(1-3), 97-111.

- Corretgé, L.G., Ugidos, J.M., Martínez, F.J., 1977. Les séries granitiques varisques du secteur centre-occidental espagnol. Collaborations internationales. CNRS, Rennes, 243, 453-461.
- Corretgé, L.G., Bea, F., Suárez, O., 1985. Las características geoquímicas del Batolito de Cabeza de Araya (Cáceres, España): implicaciones petrogenéticas. Trabajos de Geología, 15, 219-238.
- Corretgé, L.G., Castro, A., El-Hmidi, H., García-Moreno, O., 2001. Characteristics and significance of the experimental products from partial melting of rocks from the "Complejo Esquisto grauváquico" at 3.5kbar. In: III Congreso Ibérico de Geoquímica, VIII Congreso de Geoquímica de España, Zaragoza, 191-196pp.
- Corretgé, L.G., Castro, A., García-Moreno, O. 2004. Granitoides de la "serie mixta". In: Vera, J.A. (ed.). Geología de España, Sociedad Geológica Española-Instituto Geológico y Minero de España, Madrid, 115-116.
- Dall'agnol, R., Scaillet, B., Pichavant, M., 1999. An experimental study of a lower proterozoic A-type granite from the Eastern Amazonian Craton, Brazil. Journal of Petrology, 40(11), 1673-1698.
- Díaz-Alvarado, J., Castro, A., Fernández, C., Moreno-Ventas, I., 2011. Assessing Bulk Assimilation in Cordieritebearing Granitoids from the Central System Batholith, Spain; Experimental, Geochemical and Geochronological Constraints. Journal of Petrology, 52(2), 223-256.
- Diener, J.F.A., Powell, R., White, R.W., Holland, T.J.B., 2007. A new thermodynamic model for clino- and orthoamphiboles in the system Na<sub>2</sub>O-CaO- FeO-MgO-Al<sub>2</sub>O<sub>3</sub>-SiO<sub>2</sub>-H<sub>2</sub>O-O. Journal of Metamorphic Geology, 25, 631-656.
- Erdmann, S., London, D., Morgan Vi, G.B., Clarke, D.B., 2007. The contamination of granitic magma by metasedimentary country-rock material: An experimental study. Canadian Mineralogist, 45(1), 43-61.
- Fuhrman, M.L., Lindsley, D.H., 1988. Ternary-feldspar modelling and thermometry. American Mineralogist, 73, 201-215.
- García-Moreno, O., 2004. Estudio experimental de las relaciones texturales y de fases en granitos peralumínicos de la serie mixta del Macizo Ibérico. El caso de Cabeza de Araya (Cáceres). PhD Thesis. Oviedo, Universidad de Oviedo, 248pp.
- García-Moreno, O., Castro, A., Corretgé, L.G., El-Hmidi, H., 2006. Dissolution of tonalitic enclaves in ascending hydrous granitic magmas: An experimental study. Lithos, 89(3-4), 245-258.
- García-Moreno, O., Corretgé, L.G., Castro, A., 2007. Processes of assimilation in the genesis of cordierite leucomonzogranites from the Iberian massif: A short review. Canadian Mineralogist, 45(1), 71-85.
- Green, T.H.,1976. Experimental generation of cordierite- or garnet-bearing granitic liquids from a pelitic composition. Geology, 4, 85-88.
- Hall, A., Pereira, M.D., Bea, F., 1996. The abundance of ammonium in the granites of central Spain, and the behaviour of the ammonium ion during anatexis and fractional crystallization. Mineralogy and Petrology 56(1-2):105-123.

- Harley, S.L., Carrington, D.P., 2001. The distribution of H<sub>2</sub>O between cordierite and granitic melt: H<sub>2</sub>O incorporation in cordierite and its application to high-grade metamorphism and crustal anatexis. Journal of Petrology 42(9):1595-1620.
- Hensen, B.J., 1986. Theoretical phase relations involving cordierite and garnet revisited: the influence of oxygen fugacity on the stability of sapphirine and spinel in the system Mg-Fe-Al-Si-O. Contributions to Mineralogy and Petrology, 92(3), 362-367.
- Hoffer, E., Grant, J.A., 1980. Experimental investigations of the formation of Cordierite-Orthopyroxene parageneses in pelitic rocks. Contributions to Mineralogy and Petrology, 73, 15-22.
- Holland, T.J.B., Powell, R., 1996. Thermodynamics of orderdisorder in minerals. 2. Symmetric formalism applied to solid solutions. American Mineralogist, 81, 1425-1437.
- Holland, T.J.B., Powell, R., 1998. An internally consistent thermodynamic data set for phases of petrological interest. Journal of Metamorphic Geology, 16, 309-343.
- Holland, T.J.B., Powell, R., 2001. Calculation of phase relations involving haplogranitic melts using an internally consistent thermodynamic dataset. Journal of Petrology, 42, 673-683.
- Holtz, F., Johannes, W., 1991. Genesis of peraluminous granites.
  I. Experimental investigation of melt composition at 3 and 5kbar and various H<sub>2</sub>O activities. Journal of Petrology, 32(5), 935-958.
- Holtz, F., Behrens, H., Dingwell, D.B., Johannes, W., 1995. H<sub>2</sub>O solubility in haplogranitic melts: compositional, pressure and temperature dependence. American Mineralogist, 80, 94-108.
- Huang, W.L., Wyllie, P.J., 1973. Melting Relations of Muscovite-Granite to 35kbar as a Model for Fusion of Metamorphosed Subducted Oceanic Sediments. Contributions to Mineralogy and Petrology, 42, 1-14.
- Huang, W., Wyllie, P.J., 1986. Phase relations of gabbro-tonalite-granite-water at 15kbar with applications to differentiation and anatexis. American Mineralogist, 71, 301-316.
- Johannes, W., Holtz, F., 1996. Petrogenesis and experimental petrology of granitic rocks, Springer Verlag, New York, 335pp.
- Kalt, A., Altherr, R., Ludwig, T., 1998. Contact Metamorphism in Pelitic Rocks on Island of Kos (Greece, Eastern Aegean Sea): a Test for the Na-in Cordierite Thermometer. Journal of Petrology, 39(4), 663-688.
- Klimm, K., Holtz, F., Johannes, W., King, P.L., 2003. Fractionation of metaluminous A-type granites: An experimental study of the Wangrah Suite, Lachlan Fold Belt, Australia. Precambrian Research, 124(2-4), 327-341.
- Lagarde, J.L., Capdevila, R., Fourcade, S., 1992. Granites et collision: l'exemple des granitoides carboniferes dans la chaine hercynienne ouest-europeenne. Bull. Soc. geol. France, 163(5), 597-610.
- López, S., Castro, A., García-Casco, A., 2005. Production of granodiorite melt by interaction between hydrous mafic magma and tonalitic crust. Experimental constraints and implications for the generation of Archaean TTG complexes. Lithos, 79, 229-250.

- Maas, R., Nicholls, I.A., Legg, C., 1997. Igneous and metamorphic enclaves in the S-type Deddick Granodiorite, Lachlan fold belt, SE Australia: Petrographic, geochemical and Nd-Sr isotopic evidence for crustal melting and magma mixing. Journal of Petrology, 38(7), 815-841.
- Martínez, F.J., 1974. Estudio petrológico de la parte occidental de la provincia de Salamanca. Trabajos de Geología, 7, 125.
- Moore, G., Vennemann, T., Carmichael, I.S.E., 1998. An empirical model for the solubility of H<sub>2</sub>O in magmas to 3kbar. American Mineralogist, 83, 36-42.
- Nakada, S., Motomura, Y., 1999. Petrology of the 1991–1995 eruption at Unzen: effusion pulsation and groundmass crystallization. Journal of Volcanology and Geothermal Research, 89, 173-196.
- Nakamura, M., 1995. Continuous mixing of crystal mush and replenished magma in the ongoing Unzen eruption. Geology, 23, 807-810.
- Naney, M.T., 1983. Phase equilibria of rock-forming ferromagnesian silicates in granitic systems. American Journal of Science, 283, 993-1033.
- Naney, M.T., Swanson, S.E., 1980. The effect of Fe and Mg on crystallization in granitic systems. American Mineralogist, 65, 639-653.
- Oen, I.S., 1958. The geology, petrology and ore deposits of the Viseu region, Northern Portugal. Communicações dos Serviços Geologicos de Portugal, 41, 5-199.
- Oen, I.S., 1970. Granite intrusion, folding and metamorphism in central northern Portugal. Boletín Geológico y Minero, 81, 271-298.
- Parmigiani, A., Huber, C., Bachmann, O., 2014. Mush microphysics and the reactivation of crystal-rich magma reservoirs. Journal of Geophysical Research, Solid Earth, 9(8), 6308-6322.
- Patiño Douce, A.E., Beard, J.S., 1994. H<sub>2</sub>O loss from hydrous melts during fluid-absent piston cylinder experiments. American Mineralogist, 79, 585-588.
- Patiño Douce, A.E., Beard, J.S., 1995. Dehydration-melting of biotite gneiss and quartz amphibolite from 3 to 15kbar. Journal of Petrology, 36(3), 707-738.
- Pereira, M.D., Bea, F., 1994. Cordierite-producing reactions in the Peña Negra complex, Avila Batholith, Central Spain: The key role of cordierite in low-pressure anatexis. The Canadian Mineralogist, 32, 763-780.
- Pichavant, M., Costa, F., Burgisser, A., Scaillet, B., Martel, C., Poussineau, S., 2007. Equilibration scales in silicic to intermediate magmas - Implications for experimental studies. Journal of Petrology, 48(10), 1955-1972.
- Powell, R., Holland, T.J.B., 1999. Relating formulations of the thermodynamics of mineral solid solutions: Activity modelling of pyroxenes, amphiboles, and micas. American Mineralogist, 84, 1-14.
- Puziewicz, J., Johannes, W., 1988. Phase equilibria and compositions of Fe-Mg-Al minerals and melts in watersaturated peraluminous granitic systems. Contributions to Mineralogy and Petrology, 100, 156-168.

- Rapela, C.W., Baldo, E.G., Pankhurst, R.J., Saavedra, J., 2002. Cordierite and leucogranite formation during emplacement of highly peraluminous magma: the El Pilón Granite Complex (Sierras Pampeanas, Argentina). Journal of Petrology, 43(6), 1003-1028.
- René, M., Holtz, F., Luo, C., Beermann, O., Stelling, J., 2008. Biotite stability in peraluminous granitic melts: Compositional dependence and application to the generation of two-mica granites in the South Bohemian batholith (Bohemian Massif, Czech Republic). Lithos, 102(3-4), 538-553.
- Rubio-Ordóñez, A., García-Moreno, O., Montero, P., Bea, F., 2016. New data on the chronology of Cabeza de Araya Granites, (Cáceres). Geo-Temas, 16(2) 43-46.
- Sandeman, H.A., Clark, A.H., 2003. Glass-rich, cordierite-biotite rhyodacite, Valle Ninahuisa, Puno, SE Peru: Petrological evidence for hybridization of 'Lachlan S-typpe' and potassic mafic magmas. Journal of Petrology, 44(2), 355-385.
- Scaillet, B., Pichavant, M., Roux, J., 1995. Experimental crystallization of leucogranite magmas. Journal of Petrology, 36(3), 663-705.
- Scaillet, B., Holtz, F., Pichavant, M., 2016. Experimental constraints on the formation of silicic magmas. Elements, 12, 109-114.
- Schermerhorn, L.J.G., 1959. Igneous, metamorphic and ore geology of the Castro Daire-Sao Pedro do Sul-Sátao region (Northern Portugal). PhD Thesis, Amsterdam, University of Amsterdam, 517pp.
- Schmidt, M.W., 1996. Experimental constraints on recycling of potassium from subducted oceanic crust. Science, 272, 1927-1930.
- Schreyer, W., Maresch, W.V., Daniels, P., Wolfsdorff, P., 1990. Potassic cordierites: characteristic minerals for high-temperature, very low-pressure environments. Contributions to Mineralogy and Petrology, 105(2), 162-172.
- Speer, J.A., 1981. Petrology of cordierite- and almandine-bearing granitoid plutons of the southern Appalachian piedmont, U.S.A. Canadian Mineralogist, 19(1), 35-46.
- Stern, C. R., Wyllie, P. J., 1981. Phase relationships of I-type granites with H<sub>2</sub>O to 35 kbar: the Dinkey Lakes biotite-granite from the Sierra Nevada batholith. Journal of Geophysical Research, 86(b11), 10412-10422.
- Tajcmanova, L., Connolly, J.A.D., Cesare, B., 2009. A thermodynamic model for titanium and ferric iron solution in biotite. Journal of Metamorphic Geology, 27, 153-165.
- Takahashi, M., Aramaki, S., Ishihara, S., 1980. Magnetite-series/ Ilmenite-series vs. I-type/S-type granitoids. Mining Geology, Special Issue, 8, 13-28.
- Tsuchiyama, A., 1983. Crystallization kinetics in the system CaMgSi<sub>2</sub>O<sub>6</sub>-CaAl<sub>2</sub>Si<sub>2</sub>O<sub>8</sub>: the delay in nucleation of diopside and anorthite. American Mineralogist, 68, 687-698.
- Tsuchiyama, A., 1985. Crystallization kinetics in the system CaMgSi<sub>2</sub>O<sub>6</sub>-CaAl<sub>2</sub>Si<sub>2</sub>O<sub>8</sub>: development of zoning and kinetics effects on element partitioning. American Mineralogist, 70, 474-486.

- Ugidos, J.M., Recio, C., 1993. Origin of cordierite-bearing granites by assimilation in the Central Iberian Massif (CIM), Spain. Chemical Geology, 103, 27-43.
- Ugidos, J.M., Stephens, W.E., Carnicero, A., Ellam, R.M., 2008. A reactive assimilation model for regional-scale cordierite-bearing granitoids: geochemical evidence from the Late Variscan granites of the Central Iberian Zone, Spain. Earth and Environmental Science Transactions of the Royal Society of Edinburgh, 99(3-4), 225-250.
- Vielzeuf, D., Montel, J.M., 1994. Partial melting of metagreywackes. Part I. Fluid-absent experiments and phase relationships. Contributions to Mineralogy and Petrology, 117, 375-393.
- Vigneresse, J.L., Bouchez, J.L., 1997. Successive Granitic Magma Batches During Pluton Emplacement: The Case of Cabeza de Araya (Spain). Journal of Petrology, 38(12), 1767-1776.
- White, R.W., Powell, R., Holland, T.J.B., Worley, B.A., 2000. The effect of TiO<sub>2</sub> and Fe<sub>2</sub>O<sub>3</sub> on metapelitic assemblages at greenschist and amphibolite facies conditions: mineral equilibria calculations in the system K<sub>2</sub>O-FeO-MgO-Al<sub>2</sub>O<sub>3</sub>-SiO<sub>2</sub>-H<sub>2</sub>O-TiO<sub>2</sub>-Fe<sub>2</sub>O<sub>3</sub>. Journal of Metamorphic Geology, 18, 497-511.
- White, R.W., Powell, R., Holland, T.J.B., 2001. Calculation of partial melting equilibria in the system Na<sub>2</sub>O-CaO-K<sub>2</sub>O-FeO-MgO-Al<sub>2</sub>O<sub>3</sub>-SiO<sub>2</sub>-H<sub>2</sub>O (NCKFMASH). Journal of Metamorphic Geology, 19, 139-153.
- White, R.W., Powell, R., Clarke, G.L., 2002. The interpretation of reaction textures in Fe-rich metapelitic granulites of the Musgrave Block, central Australia: constraints from mineral equilibria calculations in the system K<sub>2</sub>O-FeO-MgO-Al<sub>2</sub>O<sub>3</sub>-SiO<sub>2</sub>-H<sub>2</sub>O-TiO<sub>2</sub>-Fe<sub>2</sub>O<sub>3</sub>. Journal of Metamorphic Geology, 20, 41-55.
- White, R.W., Powell, R., Holland, T.J.B., 2007. Progress relating to calculation of partial melting equilibria for metapelites. Journal of Metamorphic Geology, 25, 511-527.
- White, R.W., Stevens, G., Johnson, T.E., 2011. Is the crucible reproducible? Reconciling melting experiments with thermodynamic calculations. Elements, 7, 239-244.
- Zeck, H.P., 1992. Restite-melt and mafic-felsic magma mixing and mingling in a S-type dacite, Cerro del Hoyazo, SE Spain. Transations of the Royal Society of Edinburgh: Earth Sciences, 83, 139-144.
- Zeh, A., Holland, T.J.B., Klemd, R., 2005. Phase relationships in grunerite–garnet-bearing amphibolites in the system CFMASH, with applications to metamorphic rocks from the Central Zone of the Limpopo Belt, South Africa. Journal of Metamorphic Geology, 23, 1-17.

Manuscript received February 2017; revision accepted November 2017; published Online November 2017.

#### **ELECTRONIC APPENDIX I**

List of solution models used in the thermodynamic calculations.

The solution models used were:

- i) melt(HP) for the haplogranitic melt (Holland and Powell, 2001, improved by White *et al.*, 2001 and White *et al.*, 2007).
- ii) feldspar for plagioclase and K-feldspar (Fuhrman and Lindsley, 1988).
- iii) Pheng(HP) for muscovite (Holland and Powell, 1998)

- iv) Bio(TCC) for biotite (Tajcmanova et al., 2009).
- v) hCrd for cordierite (Holland and Powell, 1998).
- vi) Gt(WPH) for garnet (White et al., 2007).
- vii) Opx(HP) for orthopyroxene (Powell and Holland, 1999).
- viii) Cpx(HP) for clinopyroxene (Holland and Powell, 1996; Zeh *et al.*, 2005).
- ix) oAmph(DP) for orthoamphibole (Diener et al., 2007).
  - x) cAmph(DP) for clinoamphibole (Diener et al., 2007).
  - xi) Sp(WPC) for spinel (White et al., 2002).
  - xii) Ilm(WPH) for ilmenite (White et al., 2000).